VTRC
Virginia Transportation Research Council

We Bring Innovation to Transportation

Dissimilar Metal Welds Between ASTM A709 Grade 50CR and Other Bridge Steels

https://vtrc.virginia.gov/media/vtrc/vtrc-pdf/vtrc-pdf/26-R45.pdf

JASON T. PROVINES, P.E., Senior Research Scientist
Virginia Transportation Research Council

AMIR BEHRAVAN, Ph.D., P.E., Research Scientist
Virginia Transportation Research Council

MD. SOJIB HOSSAIN, Ph.D., Research Assistant
University of Virginia

SEAN R. AGNEW, Ph.D., Professor
University of Virginia

JAMES FITZ-GERALD, Ph.D., Professor
University of Virginia

STEPHEN R. SHARP, Ph.D., P.E., Associate Director
Virginia Transportation Research Council

WILLIAM MOFFAT, Ph.D., Postdoctoral Researcher
University of Virginia

Final Report VTRC 26-R45

VIRGINIA TRANSPORTATION RESEARCH COUNCIL
530 Edgemont Road, Charlottesville, VA 22903-2454
vtrc.virginia.gov

Standard Title Page - Report on Federally Funded Project

1. Report No.: FHWA/VTRC 26-R45	2. Government Accession No.:	3. Recipient's Catalog No.:
4. Title and Subtitle: Dissimilar Metal Welds Between ASTM A709 Grade 50CR and Other Bridge Steels		5. Report Date: June 2026
		6. Performing Organization Code:
7. Author(s): Jason T. Provines, Amir Behravan, Md. Sojib Hossain, Sean R. Agnew, James Fitz-Gerald, Stephen R. Sharp, and William Moffat		8. Performing Organization Report No.: VTRC 26-R45
9. Performing Organization and Address: Virginia Transportation Research Council 530 Edgemont Road Charlottesville, VA 22903		10. Work Unit No. (TRAIS):
		11. Contract or Grant No.: 120151
12. Sponsoring Agencies' Name and Address: Virginia Department of Transportation 1221 E. Broad Street Richmond, VA 23219 Federal Highway Administration 400 North 8th Street, Room 750 Richmond, VA 23219-4825		13. Type of Report and Period Covered: Final
		14. Sponsoring Agency Code:
15. Supplementary Notes: This is an SPR-B report.		

16. Abstract:

Corrosion is a prevailing cause of bridge deterioration for the Virginia Department of Transportation (VDOT) and leads to expensive maintenance actions. During the past decade, ASTM A709 Grade 50CR steel has been used on bridges to provide additional corrosion resistance, although its higher material and fabrication costs present implementation challenges. Dissimilar metal welds (DMWs) using 50CR steel in targeted, highly corrosive locations can provide enhanced corrosion protection while minimizing initial costs.

This project investigated the feasibility of using DMWs made between Grade 50CR and other bridge steels in terms of their weldability, mechanical properties, galvanic corrosion performance, and compatibility with standard nondestructive evaluation techniques. In addition, the project also sought to identify an alternative to 50CR steel because of challenges with its long lead time and quality in recent VDOT projects. ATI 412 steel was identified as a potential alternative to 50CR steel based on its similar corrosion resistance and mechanical properties. DMW specimens were fabricated by welding either 50CR or 412 steel to either ASTM A36 or ASTM A709 Grade 50W steel. A steel bridge fabricator conducted all welding by using a variety of welding parameters.

The weldability evaluation showed that DMWs made between 50CR/412 steel and A36/50W steel are susceptible to solidification cracking and cold cracking. Both types of cracking can be eliminated using lower heat input and a single-V with backgouge weld joint. Crack-free DMWs were found to meet the mechanical property requirements of the American Association of State Highway and Transportation Officials and American Welding Society (AASHTO/AWS) D1.5 Bridge Welding Code. DMWs experienced uniform, pitting, galvanic, and intergranular corrosion. Galvanic corrosion was present in the heat-affected zones on both sides of the stainless steel weld interface. The A36/50W steel heat-affected zones experienced accelerated uniform corrosion compared with the A36/50W steel base metal. The 50CR steel experienced accelerated pitting and intergranular corrosion compared with the 50CR steel base metal.

The nondestructive evaluation results showed challenges with radiographic testing, ultrasonic testing, and phased array ultrasonic testing of DMWs. Some radiographic testing conducted at the fabricator displayed artifacts that could mask potential defects in the welds. DMWs also exhibited ultrasonic anisotropic behavior and ultrasonic wave refraction, causing typical ultrasonic and phased array ultrasonic testing procedures to mislocate or completely miss defects in DMWs.

Based on the results, the Virginia Transportation Research Council recommends that VDOT not pursue using 50CR/412 steel in DMWs due to remaining challenges with their corrosion performance and nondestructive evaluation. The Virginia Transportation Research Council also recommends that VDOT continue to exercise caution with specifying 50CR steel because of recent poor quality and long lead times. Both recommendations allow VDOT to proactively manage risk on future projects and help to ensure structural integrity and on-time, on-budget project delivery.

17. Key Words: 50CR steel, corrosion, corrosion resistance, dissimilar metal welds, welding	18. Distribution Statement: No restrictions. This document is available to the public through NTIS, Springfield, VA 22161.

19. Security Classif. (of this report): Unclassified	20. Security Classif. (of this page): Unclassified	21. No. of Pages: 63	22. Price:

FINAL REPORT

DISSIMILAR METAL WELDS BETWEEN ASTM A709 GRADE 50CR AND OTHER BRIDGE STEELS

Jason T. Provines, P.E.
Senior Research Scientist
Virginia Transportation Research Council

Amir Behravan, Ph.D., P.E.
Research Scientist
Virginia Transportation Research Council

Md. Sojib Hossain, Ph.D.
Research Assistant
University of Virginia

Sean R. Agnew, Ph.D.
William G. Reynolds Professor of Materials Science
University of Virginia

James Fitz-Gerald, Ph.D.
Professor
University of Virginia

Stephen R. Sharp, Ph.D., P.E.
Associate Director
Virginia Transportation Research Council

William Moffat, Ph.D.
Postdoctoral Researcher
University of Virginia

Virginia Transportation Research Council
(A partnership of the Virginia Department of Transportation
and the University of Virginia since 1948)

Charlottesville, Virginia

June 2026
VTRC 26-R45

DISCLAIMER

The contents of this report reflect the views of the author(s), who is responsible for the facts and the accuracy of the data presented herein. The contents do not necessarily reflect the official views or policies of the Virginia Department of Transportation, the Commonwealth Transportation Board, or the Federal Highway Administration. This report does not constitute a standard, specification, or regulation. Any inclusion of manufacturer names, trade names, or trademarks is for identification purposes only and is not to be considered an endorsement.

ABSTRACT

Corrosion is a prevailing cause of bridge deterioration for the Virginia Department of Transportation (VDOT) and leads to expensive maintenance actions. During the past decade, ASTM A709 Grade 50CR steel has been used on bridges to provide additional corrosion resistance, although its higher material and fabrication costs present implementation challenges. Dissimilar metal welds (DMWs) using 50CR steel in targeted, highly corrosive locations can provide enhanced corrosion protection while minimizing initial costs.

This project investigated the feasibility of using DMWs made between Grade 50CR and other bridge steels in terms of their weldability, mechanical properties, galvanic corrosion performance, and compatibility with standard nondestructive evaluation techniques. In addition, the project also sought to identify an alternative to 50CR steel because of challenges with its long lead time and quality in recent VDOT projects. ATI 412 steel was identified as a potential alternative to 50CR steel based on its similar corrosion resistance and mechanical properties. DMW specimens were fabricated by welding either 50CR or 412 steel to either ASTM A36 or ASTM A709 Grade 50W steel. A steel bridge fabricator conducted all welding by using a variety of welding parameters.

The weldability evaluation showed that DMWs made between 50CR/412 steel and A36/50W steel are susceptible to solidification cracking and cold cracking. Both types of cracking can be eliminated using lower heat input and a single-V with backgouge weld joint. Crack-free DMWs were found to meet the mechanical property requirements of the American Association of State Highway and Transportation Officials and American Welding Society (AASHTO/AWS) D1.5 Bridge Welding Code. DMWs experienced uniform, pitting, galvanic, and intergranular corrosion. Galvanic corrosion was present in the heat-affected zones on both sides of the stainless steel weld interface. The A36/50W steel heat-affected zones experienced accelerated uniform corrosion compared with the A36/50W steel base metal. The 50CR steel experienced accelerated pitting and intergranular corrosion compared with the 50CR steel base metal.

The nondestructive evaluation results showed challenges with radiographic testing, ultrasonic testing, and phased array ultrasonic testing of DMWs. Some radiographic testing conducted at the fabricator displayed artifacts that could mask potential defects in the welds. DMWs also exhibited ultrasonic anisotropic behavior and ultrasonic wave refraction, causing typical ultrasonic and phased array ultrasonic testing procedures to mislocate or completely miss defects in DMWs.

Based on the results, the Virginia Transportation Research Council recommends that VDOT not pursue using 50CR/412 steel in DMWs due to remaining challenges with their corrosion performance and nondestructive evaluation. The Virginia Transportation Research Council also recommends that VDOT continue to exercise caution with specifying 50CR steel because of recent poor quality and long lead times. Both recommendations allow VDOT to proactively manage risk on future projects and help to ensure structural integrity and on-time, on-budget project delivery.

FINAL REPORT

DISSIMILAR METAL WELDS BETWEEN ASTM A709 GRADE 50CR AND OTHER BRIDGE STEELS

Jason T. Provines, P.E.
Senior Research Scientist
Virginia Transportation Research Council

Amir Behravan, Ph.D., P.E.
Research Scientist
Virginia Transportation Research Council

Md. Sojib Hossain, Ph.D.
Research Assistant
University of Virginia

Sean R. Agnew
William G. Reynolds Professor of Materials Science
University of Virginia

James Fitz-Gerald
Professor
University of Virginia

Stephen R. Sharp, Ph.D., P.E.
Associate Director
Virginia Transportation Research Council

William Moffat, Ph.D.
Postdoctoral Researcher
University of Virginia

INTRODUCTION

As of fiscal year 2020, the Virginia Department of Transportation (VDOT) allocates approximately $215 million per year on bridge maintenance and an additional $225 million per year on replacement or major rehabilitation of structurally deficient bridges. One major cause of these maintenance and rehabilitation efforts is corrosion. For steel bridges, corrosion damage is often not widespread across an entire bridge but rather is localized to sections of a bridge, such as beam ends under deck joints, spans over waterways with low clearance, or spans over roadways with high traffic and deicing salt application. In some cases, it can be cost effective to perform maintenance or rehabilitation of these damaged localized sections. However, in other cases, the upfront cost of mobilization for the damaged sections makes it more cost effective to perform maintenance or rehabilitation on the entire bridge.

During the past decade, about a dozen steel bridges in North America have used martensitic stainless steel, ASTM A709 Grade 50CR steel, to make steel bridges more corrosion resistant. This includes three new bridges constructed by VDOT—Route 340, Holdens Creek, and Featherbed Lane Bridge Bridges—and one instance of using 50CR steel bolted repairs on the Onancock Bridge in a corrosive environment along Virginia's Eastern Shore (Provines et al., 2023; Sharp et al., 2019). The increased use of 50CR steel is attributed to its inherent corrosion resistance, which is approximately 4 to 10 times better than that of ASTM A709 Grade 50W steel (Fletcher, 2011; Groshek and Hebdon, 2020). 50CR steel was previously referred to as ASTM A1010.

One challenge of the widespread implementation of 50CR steel is its higher material and fabrication cost relative to traditional bridge steels (Provines et al., 2023). Because of limited budgets, it can be challenging to justify the higher initial cost of using 50CR steel for repairs or for an entire bridge, even though a life-cycle cost analysis may demonstrate long-term financial savings. However, the use of dissimilar metal connections, in which 50CR steel is used only in targeted locations of a bridge girder most subject to corrosion, has the potential to minimize the amount of 50CR steel required on a project, thereby minimizing the greater upfront cost of the more corrosion-resistant material.

One potential application of a dissimilar metal connection is for the repair of corroded steel beam ends. A common repair technique for corroded beam ends is to cut out the damaged portion and weld a beam portion back in place using in-kind steel. In this example, if the existing beam were made of ASTM A36 steel, the replacement section of the beam would also be made of A36 steel. However, the repair could then be made using a dissimilar metal weld (DMW) by welding a new 50CR steel plate girder portion to the existing A36 steel beam. This procedure would allow a small amount of 50CR steel to be used in the highly corrosive area at the beam end, whereas the rest of the bridge remains coated with A36 steel.

Similarly, 50CR steel could also be used on a newly constructed bridge for portions of the girders exposed to highly corrosive environments, such as near beam ends, over water spans, or on interpass bridges over roadways with high volume and high deicing salt application. In this case, the remainder of the bridge could be fabricated with traditional uncoated 50W steel in the lesser corrosive portions to provide cost savings. Figure 1 shows a schematic highlighting what these DMW applications might look like in practice.

Although DMWs using 50CR steel have the potential to provide cost-effective corrosion resistance in targeted locations, their feasibility for bridges has not yet been determined. Their weldability is not yet known because no published data are available on DMWs, especially joining 50CR steel to other typical bridge steels. Other unknowns for such DMWs include whether structurally sound, crack-free welds can be successfully fabricated and which welding processes and parameters should be used to make these successful welds. Furthermore, if these DMWs can be successfully fabricated, it is unknown whether they can meet the mechanical property requirements necessary for use on steel bridges.

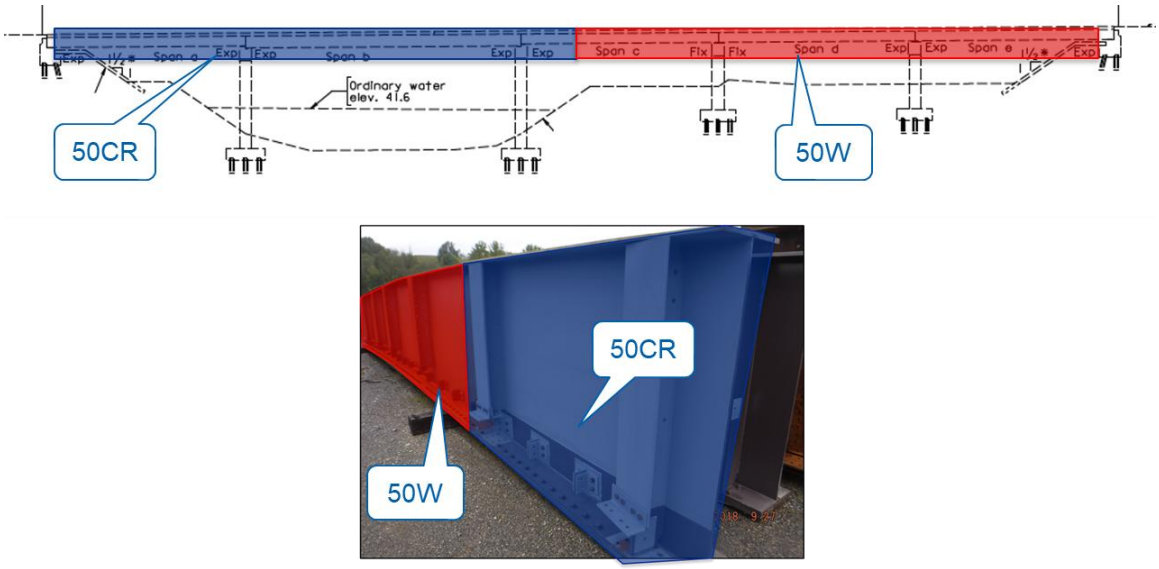

Figure 1. Schematic and Photo of Potential Applications of Dissimilar Metal Welded Steel Bridge Using 50CR Steel

In addition, the galvanic corrosion performance of DMWs made from 50CR steel and other bridge steels has been questioned. Galvanic corrosion can occur when materials with different corrosion resistance are placed in contact within a corrosive environment. For these DMWs, the 50CR steel would be joined to A36 or 50W steel using an austenitic stainless steel weld metal. This scenario means that two locations exist on such DMWs and have the potential to experience galvanic corrosion: where the 50CR steel is in contact with the stainless steel weld metal and where the A36/50W steel is in contact with the stainless steel weld metal. In both cases, the stainless steel weld metal is more corrosion resistant than either of the three base metal options, and the potential exists for galvanic reactions to accelerate corrosion of the base metals. However, it is unknown if this galvanic corrosion would be significant enough to cause concern.

It is also unknown if traditional nondestructive evaluation (NDE) techniques, such as ultrasonic testing (UT) and radiographic testing (RT) can be used for inspecting DMWs with 50CR steel. Although UT and RT are commonly used for welds made with traditional bridge steels, these techniques present additional complexities with DMWs because of the joining of three different materials (two base metals and a weld metal), all with different ultrasonic properties and response to radiography. An investigation into the NDE of DMWs is required to determine if these additional complexities still allow for accurate detection of potential flaws after welding.

While this research project was underway, VDOT also began having challenges with 50CR steel base metal. VDOT's first two 50CR steel bridges, Route 340 Bridge and Holdens Creek Bridge, were constructed in 2017 and 2022, respectively, without any major challenges from the steel supplier and fabricators (Provines et al., 2023; Sharp et al., 2019). However, VDOT experienced numerous issues on its third 50CR steel bridge, the Featherbed Lane Bridge, in 2022. The bridge had been designed with 50CR steel plate thicknesses of 1.5 inches and 3/4 inch. The lead time for the fabricator to receive these plates from the supplier was approximately

7 to 8 months. This timeframe was 1 to 2 months longer than the 6-month lead time for VDOT's previous two 50CR steel bridges and caused delays on the project.

In addition, the fabricator was required to perform procedure qualification record (PQR) tests, in accordance with the American Association of State Highway and Transportation Officials and American Welding Society (AASHTO/AWS) D1.5 Bridge Welding Code (D1.5), to verify their welding procedure. These tests require 1-inch-thick plates and must be completed with passing results prior to any production welding. Therefore, the fabricator was required to purchase a small quantity of 1-inch-thick 50CR steel plates. The lead time for this small quantity of 1-inch-thick plates was even longer than 7 to 8 months and delayed the initiation of production welding on the project.

Furthermore, once the 50CR steel was delivered from the supplier, the fabricator discovered surface cracks in an entire heat of steel. The cracks were inspected with UT, and some were measured to be 1/2 inch deep. Figure 2 shows an example of one of these cracks. Because of the widespread nature of these cracks, the entire heat of steel had to be rejected and replaced. The replacement heat of steel also had a 7- to 8-month lead time, causing further delays to the project.

Figure 2. Photograph of Crack in 50CR Steel Plate

VDOT also experienced challenges with lead times and quality on its fourth attempt at using 50CR steel on the Nottoway Spillway Bridge in 2023. Lead times on this project were 10 to 11 months and caused major delays. Some of the 50CR steel plates delivered also had significant waviness and were out of flatness tolerance prior to any welding. Figure 3 shows the severity of the waviness in the plates. The fabricator attempted to flatten the plate with heat straightening and hydraulic press fitting with tack welding, but both were unsuccessful. These quality issues with the 50CR steel caused further project delays.

In addition, the fabricator experienced seven failed PQR test results with the flux cored arc welding (FCAW) process, despite having fabricated two 50CR steel bridges in the past. The fabricator worked with both the filler metal manufacturer and an independent welding consultant but could not obtain passing test results. These challenges were attributed to a probable material issue with the 50CR steel base metal. These failed test results also led to major project delays.

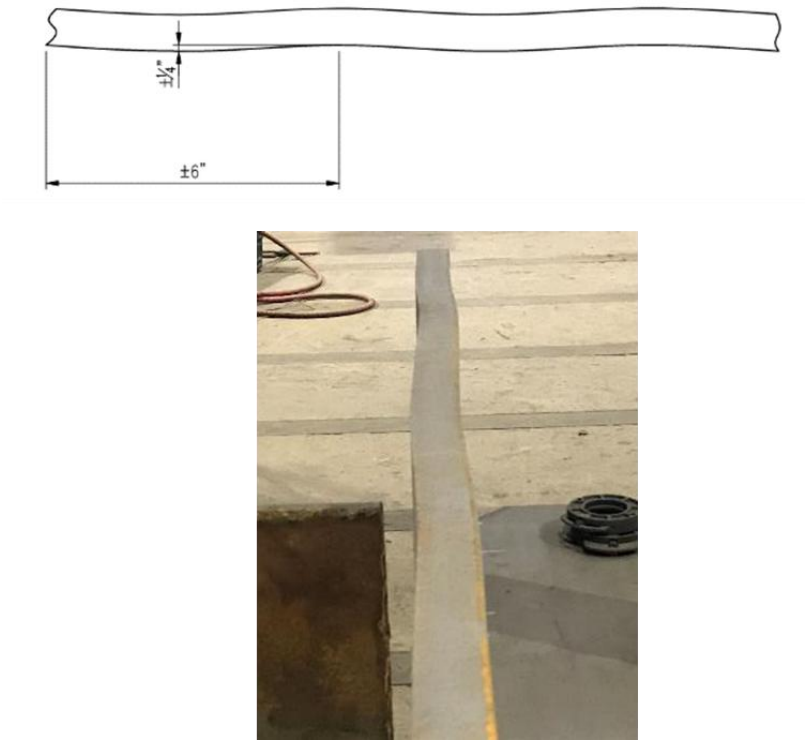

Figure 3. Schematic and Photo of Waviness in 50CR Steel Plates

Given the waviness in some plates and the lack of a solution for the failed PQR tests, VDOT elected to cancel the use of 50CR steel on the Nottoway Spillway Bridge. Table 1 shows the costs VDOT incurred because of cancelling the use of 50CR steel on the project and switching to 50W steel. As Table 1 shows, this change cost VDOT more than $1.0 million.

Table 1. Cost to VDOT Associated with Canceling Use of 50CR Steel on Nottoway Spillway Bridge

Item Description	Quantity	Unit Price	Cost Increase	Cost Decrease
50CR steel	173,300 lbs.	$ 6.85/lbs.		$ 1,187,105.00
50W steel	173,300 lbs.	$ 5.60/lbs.	$970,480.00	
Material change and impact compensation	1.0	$ 1,245,961.72	$ 1,245,961.72	
	Net Increase/Decrease:		$ 2,216,441.72	– $ 1,187,105.00
	Net Total:		$ 1,029,336.71	

Aside from the Route 340 Bridge, VDOT's other 50CR steel bridges have been fabricated by shops with limited experience in steel bridge work. VDOT's observations suggest that established bridge fabricators are reluctant to bid on 50CR steel projects because of the added risks associated with fabricating a relatively new material. At the same time, industry demand for 50CR steel remains low, providing little incentive for experienced fabricators to adapt their typical operations to include 50CR steel. Therefore, without broader adoption, less experienced fabricators or those fabricators seeking to fill capacity are likely to primarily pursue 50CR steel bridge projects, increasing the potential for fabrication challenges and project delivery risks.

Because of the challenges with the steel supplier and the large costs incurred on the Nottoway Spillway Bridge, VDOT also decided to pause future use of 50CR steel. Based on these challenges with 50CR steel and its sole supplier, it would benefit the steel bridge community if a domestically produced, readily available, high-quality alternative to 50CR steel could be identified.

PURPOSE AND SCOPE

The primary purpose of this project was to assess the feasibility of VDOT using DMWs made from joining ASTM A709 Grade 50CR steel to ASTM A36 or ASTM A709 Grade 50W steel. A secondary purpose of this project was also to identify another corrosion-resistant steel, similar to 50CR steel, for potential use in DMWs.

The scope of this research project included a literature review, specimen fabrication, weldability and metallurgical examinations, mechanical testing, corrosion testing, and NDE examination of DMWs.

METHODS

Overview

This research project consisted of the following tasks to achieve the research objective. The following lists the research tasks that are described in detail in the subsequent sections:

1. Literature review.
2. Specimen fabrication.
3. Weldability and metallurgical examination.
4. Mechanical testing.
5. Corrosion testing.
6. NDE examination.

Literature Review

The literature review focused on weldability, metallurgy, galvanic corrosion performance, and NDE of DMWs, including those welds made with 50CR steel. This effort included reviewing published reports, journal papers, and relevant specifications.

Specimen Fabrication

The research team initiated a contract with a steel bridge fabricator to have a professional welder with experience welding 50CR steel weld the DMW specimens. Table 2 shows the specimen matrix of the DMW specimens. Figure 4 shows a drawing of these DMW specimens. All these specimens were made to resemble traditional PQR plates with a groove weld in accordance with D1.5. Although traditional PQR plates are 24 inches long, these DMW specimens were fabricated to be 48 inches long to accommodate additional experimental testing.

Table 2. Specimen Matrix for Dissimilar Metal Weld Groove Welds

Group Number	Specimen Name	Thickness (in.)	Joint Type	Base Metal 1	Base Metal 2	Welding Process	Weld Filler Metal	Heat Input
1	PQR-1	7/8	SV, CSB	50CR	A36	SMAW and FCAW	309L	Typical
1	PQR-2	7/8	SV, CSB	50CR	50W	SMAW and FCAW	309L	Typical
1	PQR-3	7/8	SV, CSB	50CR	A36	SMAW and FCAW	312	Typical
1	PQR-4	7/8	SV, CSB	50CR	50W	SMAW and FCAW	312	Typical
1	PQR-9	7/8	SV, CSB	50CR	A36	SAW	309L solid	High
1	PQR-10	7/8	SV, CSB	50CR	50W	SAW	309L solid	High
1	PQR-13	7/8	SV, CSB	50CR	A36	SAW	309L solid	Typical
1	PQR-14	7/8	SV, CSB	50CR	50W	SAW	309L solid	Typical
1	PQR-15	7/8	SV, CSB	50CR	A36	SAW	309L cored	Typical
1	PQR-16	7/8	SV, CSB	50CR	50W	SAW	309L cored	Typical
2	PQR-17	7/8	SV, BG	50CR	A36	SAW	309L solid	Low
2	PQR-18	7/8	SV, BG	50CR	50W	SAW	309L solid	Low
2	PQR-19	7/8	SV, BG	50CR	A36	SAW	309L cored	Low
2	PQR-20	7/8	SV, BG	50CR	50W	SAW	309L cored	Low
3	PQR-21	1/2	SV, BG	412	A36	FCAW	309L	Low
3	PQR-22	1/2	SV, BG	412	50W	FCAW	309L	Low
3	PQR-23	1/2	SV, BG	412	A36	FCAW	312	Low
3	PQR-24	1/2	SV, BG	412	50W	FCAW	312	Low
3	PQR-25	1/2	SV, BG	412	A36	SAW	309L solid	Low
3	PQR-26	1/2	SV, BG	412	50W	SAW[a]	309L solid	Low
3	PQR-27	1/2	SV, BG	412	A36	SAW	309L cored	Low
3	PQR-28	1/2	SV, BG	412	50W	SAW	309L cored	Low

412 = 412 steel; 50CR = 50CR steel; 50W = 50W steel; A36 = A36 steel; FCAW = flux cored arc welding; PQR = procedure qualification record. SAW = submerged arc welding; SMAW = shielded metal arc welding; SV, BG = single-V with backgouge; SV, CSB = single-V with carbon steel backing. [a] Indications were found during nondestructive evaluation after original welding. Repair welds were conducted with FCAW.

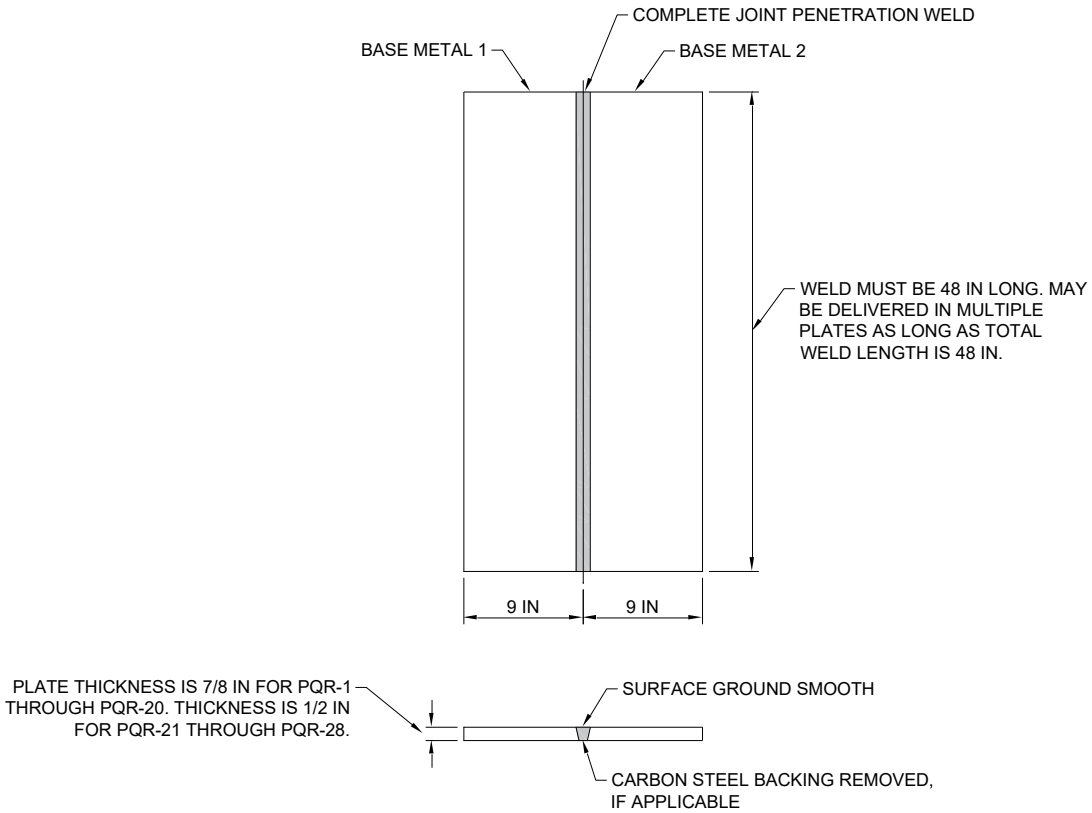

Figure 4. Drawing of Dissimilar Metal Weld Groove Weld Specimens

As Table 2 shows, these DMW specimens were categorized into three groups. The Group 1 welds were the original portion of the experimental test matrix for this testing program. All these welds used 7/8-inch-thick base metal. Typical PQR plates welded to D1.5 specifications use 1-inch-thick plates. However, VDOT owned an existing stock of 7/8-inch-thick 50CR steel from a previous bridge project, so this material was used to save costs for specimens PQR-1 through PQR-20. As Table 2 indicates, Base Metal 1 for these welds was 50CR steel, whereas Base Metal 2 was either A36 or 50W steel. 50W and A36 steels were selected because of their common use for new and older bridges, respectively.

The Group 1 welds used a single-V weld joint with a carbon steel backing plate matching Base Metal 2. Multiple welding parameters were used for these Group 1 welds, including different welding processes, weld fillers, and heat inputs. Welding processes included shielded metal arc welding (SMAW), FCAW, and submerged arc welding (SAW). As Table 2 indicates, specimens PQR-1 through PQR-4 used both SMAW and FCAW. For all four of these specimens, SMAW was used for 24 inches of weld length, whereas FCAW was used for 12 inches of weld length.

The Group 1 welds used multiple weld filler metals that were all austenitic stainless steels. Filler metals included 309L and 312 for SMAW and FCAW and both solid and cored wire versions of 309L for SAW. The 309L filler has a history of use for 50CR steel welds (Hebdon and Provines, 2020; Provines et al., 2018; Seradj, 2015; Sharp et al., 2018; 2019). The 312 filler was selected for its higher ferrite content and resistance to solidification cracking. For SAW,

solid wire 309L has been used successfully for other 50CR steel bridge welds, and cored wire 309L filler has shown favorable microstructure and mechanical properties in previous 50CR steel weld research (Fitz-Gerald et al., 2020). Multiple heat inputs were also used for different specimens to evaluate welding productivity.

The Group 2 weld parameters were modified to address cracking issues experienced in the Group 1 welds. Additional details of these cracking issues will be discussed further in this report. The Group 2 welds used a different weld joint geometry and low heat input and focused only on the SAW process. These Group 2 welds used a single-V with backgouge joint geometry, eliminating the need for the carbon steel backing plate. The Group 2 welds were focused on SAW because this welding process produced the most severe cracking in the Group 1 welds.

The Group 3 welds focused on ATI 412 steel, which is a potential alternative to 50CR steel. Like 50CR steel, 412 steel is a martensitic stainless steel and is produced by a domestic steel supplier. 412 steel has similar chemistry to 50CR steel and, thus, was expected to provide similar corrosion resistance. It also has similar mechanical properties to 50CR steel, including yield strength, tensile strength, and Charpy V-notch (CVN). However, whereas 50CR steel gets its mechanical properties from heat treatment, 412 steel gets its mechanical properties from alloying. For this reason, 412 steel does not meet the heat treatment requirements for 50CR steel in ASTM A709. The supplier also indicated that 412 steel is produced regularly and that the expected lead time is approximately 2 months.

The Group 3 welds used the same weld joint and heat input as the Group 2 welds because these modifications solved the cracking issues. These welds were performed using both FCAW and SAW processes.

The bridge fabricator conducted RT and UT as part of their acceptance testing prior to shipping the specimens to the research team. RT considered both film and digital techniques and was evaluated based on welds subject to tension following Virginia Test Method-29 for Radiographic Inspection of Groove Welds. UT followed Virginia Test Method-30 for Ultrasonic Inspection of Groove Welds (VDOT, 2018). During welding and NDE, all notable test reports, notes, and observations were to be provided to the research team. All welding and fabrication of these specimens were to meet the requirements of VDOT's special provision for 50CR steel.

Weldability and Metallurgical Examination

Several characterization techniques were used to assess the metallurgical attributes of different weld regions of the DMW specimens, including optical microscopy, scanning electron microscopy (SEM), energy dispersive spectroscopy (EDS), X-ray fluorescence, and electron backscatter diffraction. In general, data were collected multiple times from different samples taken from different locations along the length of each DMW specimen. All measurements were conducted under standard operating conditions of temperature and pressure.

For metallographic analysis, the samples were polished with a series of increasingly finer abrasive papers, followed by final polishing using a 1 micron diamond slurry. The A36 and 50W

steels were etched with 2% nital, and the 50CR steel samples were etched using Vilella's reagent.

Macro-etching was performed using three different etching reagents applied through the swabbing technique. The three different etching reagents used were 2% nital for the A36 and 50W steels, Vilella's reagent for 50CR steel, and Glyceregia to reveal the delta ferrite in the fusion zone of each weld.

Hardness measurements were performed using the Vickers scale.

Mechanical Testing

The mechanical testing for the DMW groove weld specimens included the tests indicated in Table 3.

Table 3. Mechanical Tests Conducted on Dissimilar Metal Weld Groove Weld Specimens

Mechanical Test	# Specimens from Each Groove Weld Plate	Properties Measured
Side-bend	2	Soundness and ductility
Reduced section tension	2	Tensile strength
All weld-metal tension	1	Tensile strength, yield strength, and ductility
Charpy V-notch	5	Relative fracture toughness

The mechanical test specimens were cut out from the larger DMW groove weld specimens using a water jet. Figure 5 shows an example of the orientation of the metallurgical, mechanical, and corrosion test specimens relative to the larger DMW groove weld plate. All the mechanical tests were conducted in accordance with the test procedures described in D1.5.

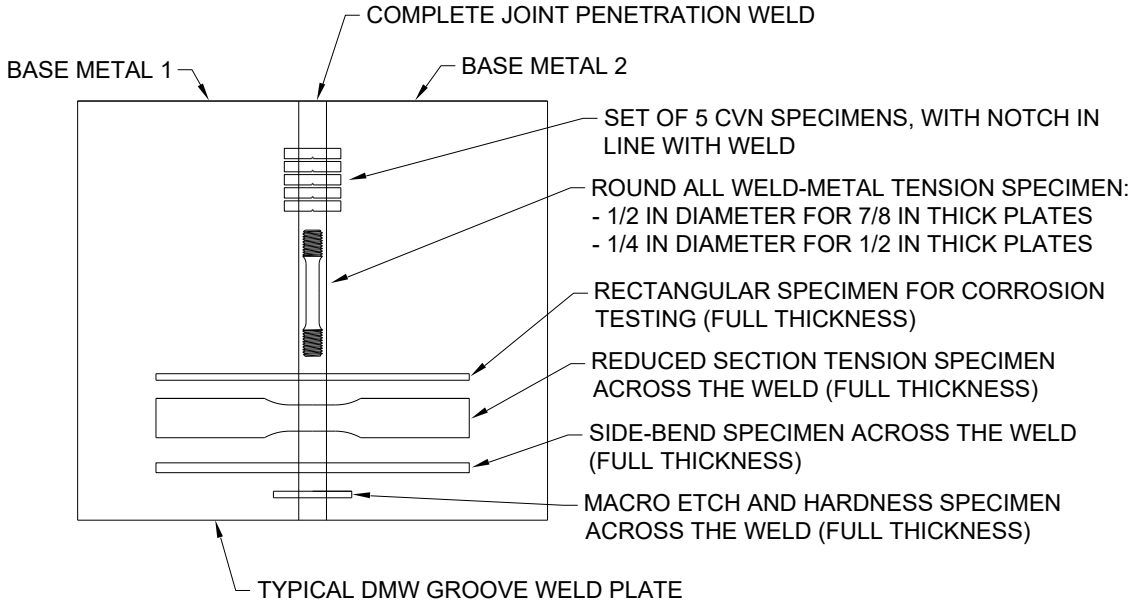

Figure 5. Orientation of Metallurgical, Mechanical, and Corrosion Samples from Dissimilar Metal Weld Specimens. CVN = Charpy V-notch; DMW = dissimilar metal weld.

Corrosion Testing

As Table 2 indicates, many different variables were evaluated in this project. Some of those variables included different base metals being joined with different filler metals while subjected to different heat inputs during welding. All these variables and others can strongly influence the resulting microstructures of the heat-affected zones (HAZs), which affects the corrosion behavior of these DMWs. The A36 and 50W steels were expected to exhibit more uniform corrosion evenly across their surfaces, whereas the 50CR steel, 309L weld metal, and HAZs were expected to exhibit more localized corrosion in selected areas.

Corrosion testing included both uniform and localized corrosion test methods to ensure multiple types of corrosion behaviors were evaluated. Overall, tests consisted of the following: saltwater droplet, accelerated corrosion chamber, partial immersion, and electrochemistry testing. The following sections describe the test methods for each of these three types of tests.

Saltwater Droplet Testing

The saltwater droplet testing procedure was devised to be a "medium-term" test procedure, opposed to accelerated corrosion chamber testing conducted during 2 to 3 months and long-term testing conducted during multiple years, such as placing corrosion samples out in the field for monitoring. Only DMWs that produced good weldability and passed the mechanical test requirements were subject to the saltwater droplet testing. No DMWs made with 412 steel were included in the saltwater droplet testing because of project time constraints. The DMW specimens tested included four samples each of specimens PQR-17 through PQR-20.

The saltwater droplet testing consisted of placing corrosion samples into waterproof enclosures for a period of 6 months. The enclosures had fully saturated (i.e., 100%) sodium chloride (NaCl) saltwater solution baths inside to provide saltwater air, and constant humidity was maintained in reference to the ASTM E104 standard. The enclosure lids maintained roughly constant humidity throughout the test. Additional water and salt were added to the baths as necessary during testing. DMW corrosion specimens were placed on top of the saltwater bath containers.

In addition, saltwater droplets from a 5% by weight NaCl solution were applied weekly to the tops of the DMW corrosion specimens in multiple locations. In general, one saltwater droplet was applied to three locations on the bulk carbon steel portion of the samples, one droplet was applied at each side of the weld interface with the base metal, and one was applied to three locations on the 50CR steel. Eight saltwater droplets in total were applied to each DMW sample weekly for 6 months. Figure 6 shows the test setup for the saltwater droplet corrosion testing.

After 6 months of testing, the DMW corrosion samples were removed from the enclosures and cut into cross sections at each saltwater droplet location (Figure 7). The cross sections were then examined under a microscope. The depth and width of each corrosion pit in the cross section were then measured and recorded (Figure 8).

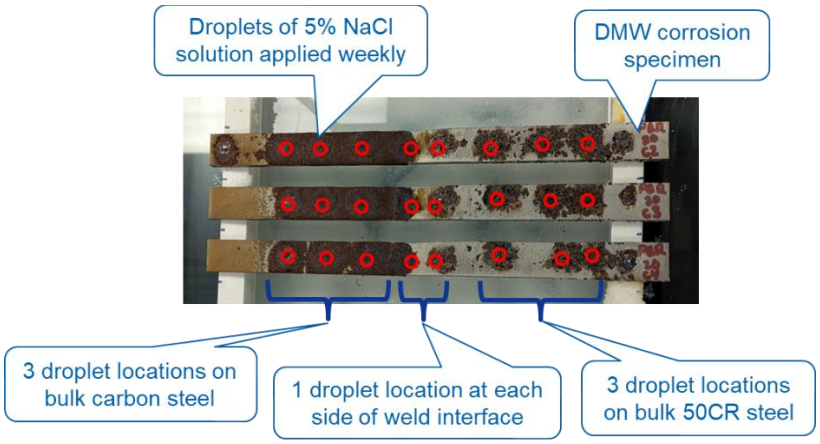

Figure 6. Example of Test Samples for Saltwater Droplet Testing of DMW Corrosion Specimens. DMW = dissimilar metal weld.

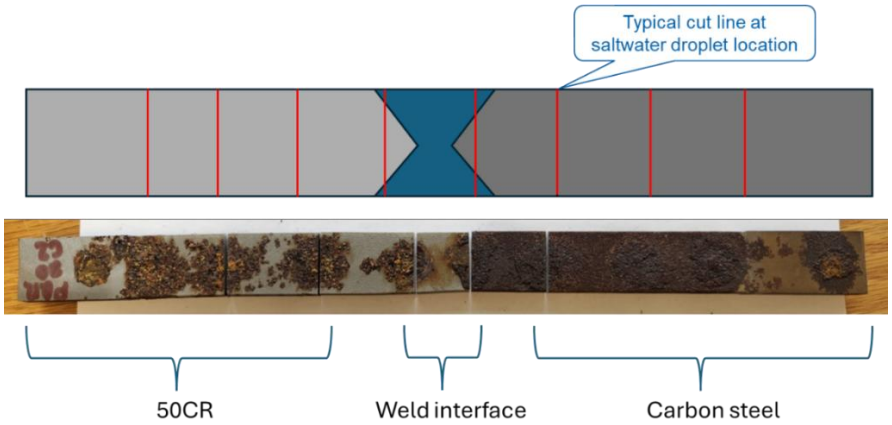

Figure 7. Diagram and Photo Showing Cut Line Locations for Saltwater Droplet Testing

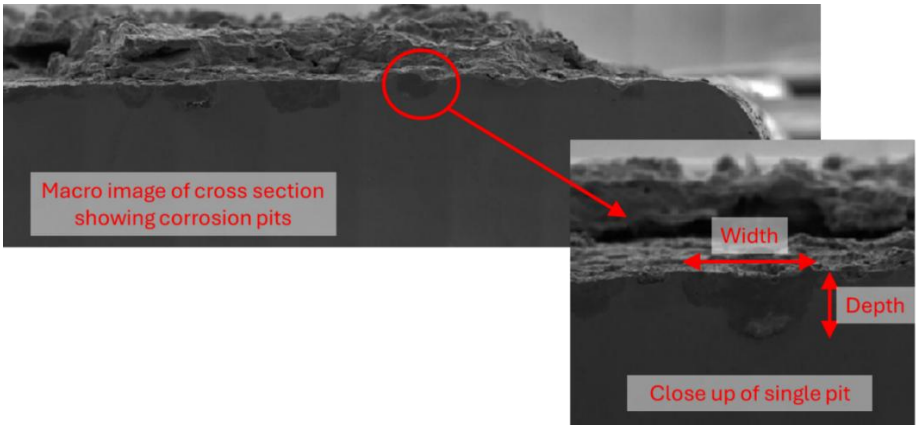

Figure 8. Macro Image and Close-up of Corrosion Pits and Measurements during Saltwater Droplet Testing

Accelerated Corrosion Chamber Testing

The accelerated corrosion chamber was conducted to provide a relative comparison of different base metals and DMW specimen types in an aggressive corrosive environment, which might occur after multiple seasons of deicing roadways under bridges. A Federal Highway

Administration-sponsored study demonstrated that deicing salt solutions can reach into the steel girder area because of vehicles passing under the bridge (Lottes and Bojanowski, 2013). Accelerated corrosion chamber testing included all the DMW specimens, which had good weldability and passed the mechanical testing requirements, including all the Group 3 weld specimens made using 412 steel. Additional base metal samples were tested for comparison. Altogether, three replicates of the following sample types were subject to accelerated corrosion chamber testing: A36 steel, 50W steel, 50CR steel, PQR-1, PQR-2, and PQR-17 through PQR-28.

The accelerated corrosion chamber testing followed a modified SAE J2334 test procedure similar to that used in previous 50CR steel base metal and galvanic corrosion testing (Fletcher, 2011; Groshek and Hebdon, 2020; SAE International, 2016). In general, that test method involved subjecting corrosion specimens to repeated cycles of three stages: humidity, salt solution application, and drying. Specimens in this project underwent 80 cycles of accelerated corrosion chamber testing.

In previous similar corrosion testing on 50CR steel, specimens were placed in the accelerated corrosion test chamber at an angle of 15° from vertical (Fletcher, 2011; Groshek and Hebdon, 2020). However, for this project, all specimens were placed horizontally. This maneuver was performed to mimic the orientation of the bottom flange of a bridge girder, but was also expected to produce more severe corrosion behavior compared with testing in the literature.

After the accelerated corrosion chamber testing was complete, the specimens were removed from the chamber. They were then blast cleaned in accordance with ASTM G1 (ASTM International, 2017), using #80 grit garnet blast media and 100 psi air pressure to remove the tightly adherent corrosion layer on the specimens. Care was taken to stop blasting the specimens immediately on reaching the base metal.

Partial Immersion Testing

To assess the corrosion behavior of the DMWs in a realistic, representative environment in which a bridge could be located, weld cross sections were placed in a petri dish immersed halfway in a saltwater solution (NaCl 3.5 wt.%). By placing one-half of the sample immersed in the solution, fully submerged regions of the samples, as well as air-exposed regions at the air-water meniscus, could be tested simultaneously. These samples were removed and photographed at set time intervals to document the appearance of the DMWs after exposure. SEM images were also captured of the corroded sample areas.

Electrochemistry Testing

Corrosion measurements were made on each of the base metals and DMW samples. These samples included the following baes metals: Grade 36, 50W steel, 50CR steel, and 309L weld metal. It also included the following welded samples: Grade 36 with 309L weld metal, 50W steel with 309L weld metal, and 50CR steel with 309L weld metal. Welds were cross-sectioned and mechanically polished to 1200 grit using silicon carbide polishing paper, and then

electrochemical measurements were performed using 3.5 wt.% NaCl solution. Electrochemistry testing included:

- Open circuit potential (OCP) to determine relative anode and cathode behavior when these samples are subjected to saltwater solutions. This work was performed in accordance with ASTM G82 (ASTM International, 1981).
- Potentiodynamic polarization to evaluate pitting and galvanic tendencies when these samples are subjected to saltwater solutions. The experiments were conducted in accordance with ASTM G5 (ASTM International, 2021a).
- Galvanic current measurement using a zero resistance ammeter (ZRA) to evaluate the galvanic polarization and current (corrosion rate) when these samples are subjected to saltwater solutions. The experiments were conducted in accordance with ASTM G71 (ASTM International, 2019). ZRA is commonly used to experimentally investigate the effects of galvanic corrosion in welds (Okonkwo et al., 2019; 2021).
- Partial immersion testing was performed to confirm corrosion behaviors when subjected to water pooling during field conditions.

The electrochemistry test samples were also evaluated after testing for chromium concentration sensitivity and intergranular attack. Whenever chromium is added to steel to improve its corrosion resistance, it can cause the corrosion mechanism to change from a predictable, uniform corrosion loss to an unpredictable mechanism, such as pitting or cracking. Fortunately, if an alloyed steel is properly selected for a given corrosive environment, uniform and localized corrosion of the structural member can be mitigated and an acceptable service life achieved. (Fletcher, 2011). Post-test characterization for chromium sensitivity and intergranular attack included unaided visual analysis, optical microscopy, SEM, and EDS.

Nondestructive Evaluation Examination

The NDE examination in this project included the following subtasks:

- Evaluating how temperature affects the acoustic properties—specifically ultrasonic wave velocity—of various materials during UT of DMWs.
- Assessing the reliability of phased array ultrasonic testing (PAUT) for detecting defects in DMWs.
- Investigating the accuracy of alternating current field measurement (ACFM) as an NDE method for identifying surface defects in steel bridge welds.

Ultrasonic Wave Velocity Testing

For ultrasonic wave velocity testing, rectangular prismatic steel specimens were prepared from A36, 50CR, and 412 steel materials. In addition, a pure 309L weld metal sample was extracted from a DMW specimen made with 50CR and A36 steels. Table 4 summarizes the dimensions of all samples. The samples were subjected to different temperatures, and the wave velocity was measured at each temperature. To measure the wave velocity, a Proceq Flaw Detector 100 ultrasonic instrument was used in combination with a 5 MHz mono probe from Sonatest. By calibrating the measuring equipment to the P-wave velocity in the steel samples at

various temperatures—and using the known sample thickness along with identifying signal peaks corresponding to the top and back surfaces—the wave velocity at each temperature could be accurately determined.

Table 4. Dimensions of Ultrasonic Testing Specimens

Steel Type	Length (in.)	Width (in.)	Thickness (in.)
50CR steel	2	2	0.875
A36 steel	2	2	0.875
412 steel	2	2	0.54
Pure 309L weld metal	1.03	0.26	0.86

Phased Array Ultrasonic Testing and Alternating Current Field Measurement Testing

Three NDE specimens were prepared for PAUT and ACFM testing. Each specimen contained a DMW, 50CR steel base metal, and either A36 or 50W steel base metal. Table 5 summarizes detailed information on each specimen.

Table 5. Details of Phased Array Ultrasonic Testing and Alternating Current Field Measurement Specimens

Specimen Name	Thickness (in.)	Base Metal 1	Base Metal 2	Weld Process	Weld Filler Metal
NDE-1	7/8	50CR	A36	SAW	309L solid
NDE-2	7/8	50CR	50W	SAW	309L solid
NDE-3	7/8	50CR	50W	SAW	309L cored

NDE = nondestructive evaluation; SAW = submerged arc welding.

Known defects were introduced into each base metal at varying depths from the surface, along with multiple defects in the weld metal and at the weld or base metal interface. In addition, three notches were created on the surface of the samples to simulate surface cracks; however, these notches were intentionally shallow. Figure 9 shows a schematic view of the NDE specimens.

Data were collected using a Cypher 64:128PR TFM64 instrument equipped with a shear wave wedge probe, featuring a 5 MHz frequency and 64 elements. The plates were examined using a start angle of 40° and a stop angle of 70°. In addition, a longitudinal dual matrix probe, featuring 4 MHz and 2 x 32 elements, was used with the Gekko 64:128PR TFM 128 instrument for comparison. Figure 10 shows the probes used for this testing.

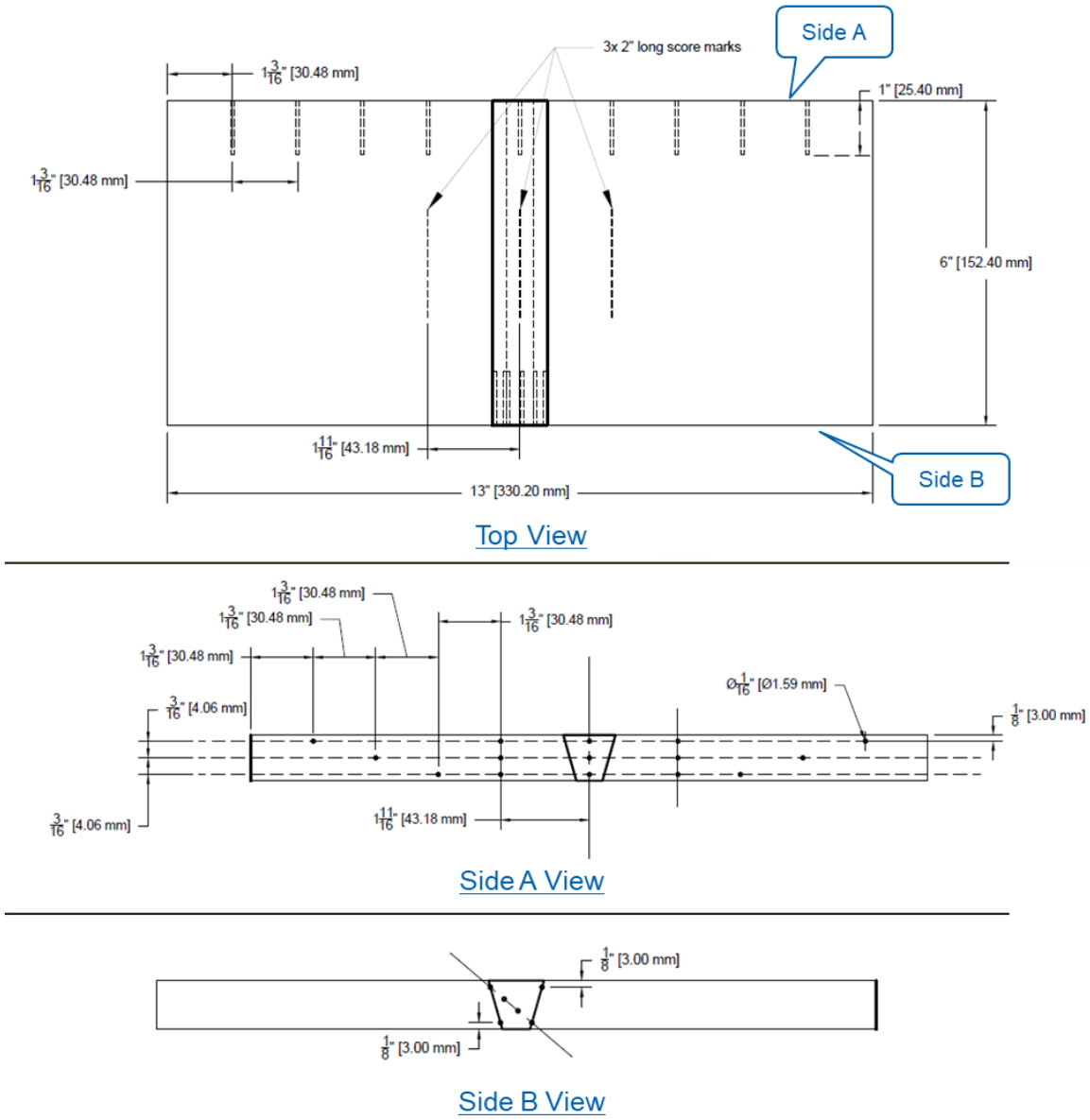

Figure 9. Schematic View of the Nondestructive Evaluation Specimens with Known Defects for Nondestructive Testing, Showing Top and Side Views

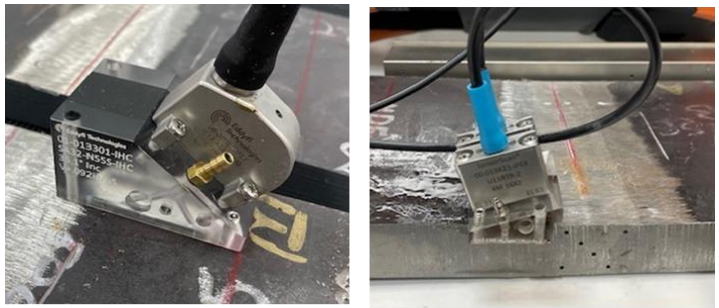

Figure 10. Wedge Probes Used for Testing Nondestructive Evaluation Specimens

RESULTS AND DISCUSSION

Literature Review

Weldability and Mechanical Properties

An appropriate filler metal must be used to effectively fabricate DMWs made with 50CR steel and A36/50W steel. The 309L filler metal exhibits a dual-phase austenitic-ferritic structure and provides excellent corrosion and oxidation resistance in marine and high-temperature environments (Khan and Chhibber, 2020). Alternatively, the 312 filler metal offers high tensile strength and exceptional corrosion resistance (Murat and Basyigit, 2020). Table 6 presents the detailed chemical compositions of the base and filler metals examined in this project.

Table 6. Chemical Composition of Base and Filler Metals

Steel Type	Elements (wt.%)										
	C	Mn	P	S	Si	Ni	Cr	Cu	V	N	Mo
A36	0.25	0.80–1.20	0.04 max.	0.05 max.	0.40 max.			0.20			
50W	0.19 max.	0.80–1.25	0.030 max.	0.030 max.	0.30–0.65	0.40 max.	0.40–0.65	0.25–0.40	0.02–0.10		
50CR	0.030 max.	1.50 max.	0.040 max.	0.010 max.	1.00 max.	1.50 max.	10.5–12.5			0.030 max.	
309L	0.03 max.	1.0–2.5	0.04 max.	0.03 max.	0.30–0.65	12.0–14.0	23.0–25.0	0.75 max.			0.75 max.
312	0.15 max.	1.0– 2.5	0.03 max.	0.03 max.	0.30–0.65	8.0–10.5	28.0–32.0	0.75 max.			0.75 max.

Max = maximum.

Welding induces significant thermal gradients across a weld joint, especially affecting the HAZs of the base metals. Variations in thermal expansion, diffusion, and phase transformation across the weld interface lead to changes in microstructure, hardness, and residual stress, affecting both mechanical properties and corrosion performance (Easterling, 1992).

Differences in physical properties and solidification behavior between stainless and carbon steels in DMWs can lead to hot and cold cracking. Hot cracking occurs during welding and is more frequent than other forms of cracking. It is also particularly detrimental to mechanical properties. Hot cracking is commonly termed solidification cracking. Cracks typically form near the centerline of the weld pass because of the segregation of elements with different melting points (Figure 11). The formation of these cracks during solidification then causes tensile stresses to develop across the weld joint.

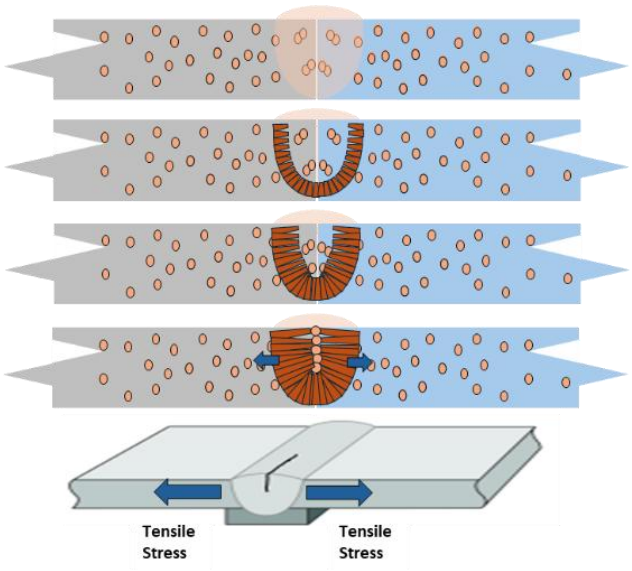

Figure 11. Schematic Showing the Formation of Solidification Cracking due to Segregation of Low-Melting Point Elements

Previous studies on the welding of carbon steel to other martensitic stainless steels, such as 50CR steel, have reported martensite and carbide formation at the fusion boundary, leading to increased cold cracking susceptibility (Khorrami et al., 2014). Other welding research studies have identified brittle martensite, residual stress, and thermal mismatch as causes of hot and cold cracking (Alcantar-Modragon et al., 2021).

Galvanic Corrosion

Although no publications have documented the galvanic corrosion behavior of 50CR steel in *welded* connections, two studies have been conducted on the galvanic corrosion behavior of 50CR steel in *bolted* connections. One study used ZRA testing, following the principles of ASTM G71 (ASTM International, 2019), to test coupons taken from 50CR steel plates, 50W steel plates, and hot-dipped galvanized (HDG) ASTM F3125 Grade A325 (Grade A325) bolts (Zhang et al., 2019). Pairs of coupons were then placed in a saltwater solution (either 0.1% for light saline exposure or 3.5% for heavy saline exposure) and connected through a ZRA to measure their galvanic corrosion current and galvanic corrosion potential.

The light saline exposure test results showed that the 50CR steel and HDG Grade A325 bolt pairing performed similarly to the 50W steel and HDG Grade A325 bolt pairing (Zhang et al., 2019). However, the heavy saline exposure results showed that the 50CR steel and HDG Grade A325 bolt pairing exhibited much more severe results than the 50W steel HDG Grade A325 bolt pairing. For the 50CR steel and HDG Grade A325 bolt pairing, the zinc on the HDG Grade A325 bolt was completely consumed. The now uncoated Grade A325 bolts continued to corrode at an accelerated rate for the remainder of the test. The study concluded that HDG Grade A325 bolts should not be used with 50CR steel in highly corrosive environments.

Virginia Tech also conducted a study investigating the galvanic corrosion performance of 50CR steel bolted to other ASTM A709 (A709) steels, including Grade 50, 50W, and HDG

Grade 50 (Groshek and Hebdon, 2020). This study used the modified SAE J2334 corrosion test procedure, which is the same as used for the current project. Both base metal specimens and bolted connection specimens were evaluated in this study. Bolted connection specimens consisted of two different types of steels connected via a nylon bolt. In some cases, these two different steel types were directly connected, and in other cases, a nylon barrier was used between them. This step was performed to evaluate galvanic corrosion. Table 7 shows the thickness losses for the different types of steel included in the study.

Table 7. Galvanic Corrosion Thickness Losses of 50CR and Other ASTM A709 Steels in Virginia Tech Corrosion Testing

Steel Type	Connection Type	Thickness Loss of Micron per Cycle			
		Cycles 0–20	Cycles 0–60	Cycles 60–80	Cycles 0–80
50CR steel	Base metal with no connection				0.53
Grade 50	Base metal with no connection				6.02
50W steel	Base metal with no connection				5.42
HDG Grade 50	Base metal with no connection				0.56
50CR steel	Directly connected to Grade 50	1.46		3.25	
50CR steel	Nylon barrier between Grade 50	1.95		4.41	
50CR steel	Directly connected to 50W steel	1.80		4.15	
50CR steel	Nylon barrier between 50W steel	1.79		4.03	
50CR steel	Directly connected to HDG Grade 50		0.85		
50CR steel	Nylon barrier between HDG Grade 50		1.44		
Grade 50	Directly connected to 50CR steel				8.93
Grade 50	Nylon barrier between 50CR steel				8.39
50W steel	Directly connected to 50CR steel				9.09
50W steel	Nylon barrier between 50CR steel				8.06
HDG Grade 50	Directly connected to 50CR steel		2.68		
HDG Grade 50	Nylon barrier between 50CR steel		1.62		

HDG = hot-dipped galvanized.

The base metal results (the first four rows of Table 7) showed that 50CR steel had a thickness loss about 10 to 11 times less than Grade 50 or 50W steel (Groshek and Hebdon, 2020). The thickness loss of 50CR steel was only slightly better than that of the HDG Grade 50.

For the bolted connection specimens (the last 12 rows of Table 7), the thickness losses of the 50CR steel when connected to Grade 50 or 50W steel increased during the course of the test, so thickness losses were reported for different cycle counts (Groshek and Hebdon, 2020). Overall, the thickness loss in the bolted connections of the 50CR steel was greater than that in the 50CR base metal specimens and was attributed to crevice corrosion. The thickness losses of the other A709 steels were also greater than their respective base metal specimens. This scenario showed that bolted connections with 50CR steel will cause galvanic corrosion to the A709 steel, including HDG to be consumed after 60 cycles of testing for the HDG Grade 50 steel. Crevice corrosion was observed to increase the thickness loss of all A709 steels.

Nondestructive Evaluation

Stainless steels have complex microstructures. They are both inhomogeneous and anisotropic, making ultrasonic wave propagation challenging (Han et al., 2015; Kumar et al., 2013). In addition, these steels have large grain sizes, which introduce several significant challenges during UT, including the following:

- A reduction in signal-to-noise ratio or an increase in backscattered energy (Edelmann, 1981; Kumar et al., 2013).
- Greater attenuation of ultrasonic waves, which shortens the effective inspection range (Nageswaran et al., 2009).
- Increased distortion or skewness during wave propagation (Chassignole et al., 2009; Edelmann, 1991; Kumar et al., 2013).

PAUT uses refraction and mode conversion at the interface between the ultrasonic wedge and the test surface to generate a shear wave at a specific incident angle (Connor et al., 2019; Schroeder et al., 2021). However, minor variations in shear wave velocity can significantly deviate the refracted beam angle, potentially leading to inaccurate flaw positioning or misclassification of defects (Connor et al., 2019; Schroeder et al., 2021). Although PAUT offers broader inspection coverage compared with conventional UT, this increased coverage does not guarantee the detection of all discontinuities within the inspected area (Connor et al., 2019).

D1.5 requires UT or RT, or both, of complete joint penetration welds. At present, most tension bridge welds are inspected solely using RT, whereas fracture-critical welds undergo both RT and UT (Connor et al., 2019). Generally, UT methods have shown increased sensitivity to crack-like flaws, whereas RT methods have shown increased sensitivity to volumetric flaws (Connor et al., 2019).

The advantages of RT include providing a visual image of the results and being applicable to a wide range of materials. However, RT also has several disadvantages, including safety, difficulty in automating, and not providing information about the depth of surface flaws. Moreover, like UT, large grain structures are a challenge for RT, potentially obscuring the image and hindering flaw detection. In traditional RT, the presence of numerous film artifacts, scratches, and poor contrast makes inspection challenging. Presently, digital radiographic images are used for identifying flaw locations and measuring their lengths. Even when RT is performed correctly, interpretation errors can still occur, including missing existing defects or misclassifying identified flaws. The RT inspection relies heavily on the inspector's judgment and demands significant experience, keen eyesight, and thorough knowledge of the techniques used.

In steel fabrication shops, the UT calibration process is typically conducted using a standard reference block stored in a room at a temperature different from the workshop where production welding is performed. However, if the acoustic properties of the reference block differ from the acoustic properties of the actual material being tested, it can lead to inaccuracies in detecting and classifying flaws. Using a unique IIW-type calibration block outlined in D1.5 for all metals can result in missing weld defects, incorrect ratings or locations, and false calls that require unnecessary repairs. Both the International Organization for Standardization (ISO) and

the American Society of Mechanical Engineers (ASME) specify that calibration must be adjusted when differences are observed in material attenuation between the calibration block and the test specimen, including variations in both the base metal and weld metal (ASME, 2017; ISO, 2012). The change in sound velocity at different temperatures is overlooked in the literature, which needs further investigation to assess their effect on acoustic properties and, if necessary, consider appropriate UT temperature correction factors.

Specimen Fabrication

The steel bridge fabricator welded all the DMW specimens. Table 8 shows the weld filler metal products used for the DMW groove weld specimens. Lincoln 880M flux was used for all the SAW welds. One hundred percent CO_2 shielding gas was used for all FCAW.

Table 8. Weld Filler Products Used for Dissimilar Metal Weld Groove Weld Specimens

Welding Process	Filler Metal Type	Filler Metal Product Name
SMAW	309L	Arcos 309L-16
SMAW	312	Arcos 312-16
FCAW	309L	SelectAlloy 309L-AP
FCAW	312	SelectAlloy 312-AP
SAW	309L solid	Arcos 309L
SAW	309L cored	SelectAlloy 309L-C

FCAW = flux cored arc welding; SAW = submerged arc welding; SMAW = shielded metal arc welding.

Table 9 shows the actual welding parameters used for the DMW specimens. Empty entries in Table 9 indicate that the fabricator did not provide a parameter. Note the decrease in the maximum interpass temperature, average interpass temperature, and heat input from the Group 1 to Group 2 specimens. These values decreased because of cracking found in the Group 1 welds, which the Weldability and Metallurgical Examination section of this report will discuss. The preheat was between 150 and 200°F for all the DMW groove weld specimens. The voltage was 28 V for SMAW and FCAW specimens and 30 V for SAW specimens. The amperage for the SMAW and FCAW specimens was an average of 155 amps. The estimated travel speed was 18 inches per minute for Group 1 specimens and 20 inches per minute for Group 2 and 3 specimens. All the specimens had approximately 8 to 15 weld passes.

The preheat was between 150 and 200°F for all the DMW groove weld specimens. The voltage was 28 V for SMAW and FCAW specimens and 30 V for SAW specimens. The amperage for the SMAW and FCAW specimens was an average of 155 amps. The estimated travel speed was 18 inches per minute for Group 1 specimens and 20 inches per minute for Group 2 and 3 specimens. All the specimens had approximately 8 to 15 weld passes.

Table 9. Actual Welding Parameters Used for the Dissimilar Metal Weld Groove Weld Specimens[a]

Group Number	Specimen Name	AASHTO/AWS D1.5 Joint Detail	Maximum Interpass Temperature (°F)	Average Interpass Temperature (°F)	Average Heat Input (kJ/in.)	Radiographic Testing Notes
1	PQR-1	B-U2a (1/4” @ 45°)	450	225	20	Multiple slag inclusions and lack of fusion
1	PQR-2	B-U2a (1/4” @ 45°)			20	
1	PQR-3	B-U2a (1/4” @ 45°)	300	250	20	Multiple layers of cracks and slag inclusions
1	PQR-4	B-U2a (1/4” @ 45°)			20	
1	PQR-9	B-U2-S (5/8” @ 20°)	445	345	59.8	Full-length subsurface crack and surface crack
1	PQR-10	B-U2-S (5/8” @ 20°)				Full-length crack
1	PQR-13	B-U2-S (5/8” @ 20°)	300	215	40.2	Crack
1	PQR-14	B-U2-S (5/8” @ 20°)	275	220	42.6	
1	PQR-15	B-U2-S (5/8” @ 20°)	325	250	36.2	Clean, corncob appearance
1	PQR-16	B-U2-S (5/8” @ 20°)	325	220	36.2	Clean, corncob appearance
2	PQR-17	B-L2c-S (0” @ 60°)	250	250	31.5	Clean, corncob appearance
2	PQR-18	B-L2c-S (0” @ 60°)	250	250	31.5	Clean, corncob appearance
2	PQR-19	B-L2c-S (0” @ 60°)	250	250	31.5	Clean, corncob appearance
2	PQR-20	B-L2c-S (0” @ 60°)	250	250	31.5	Clean, corncob appearance
3	PQR-21	B-U2-GF (01/8” @ 60°)				
3	PQR-22	B-U2-GF (0-1/8” @ 60°)				
3	PQR-23	B-U2-GF (0-1/8” @ 60°)				
3	PQR-24	B-U2-GF (0-1/8” @ 60°)				
3	PQR-25	B-L2c-S (0” @ 60°)				Flaw
3	PQR-26	B-L2c-S (0” @ 60°)				Flaw
3	PQR-27	B-L2c-S (0” @ 60°)				
3	PQR-28	B-L2c-S (0” @ 60°)				

AASHTO = Association of State Highway and Transportation Officials; AWS = American Welding Society; PQR = procedure qualification record. [a] Blank cells indicate that no data were provided.

The welder from the fabricator stated that welding the Group 1 specimens was much easier with FCAW than with SMAW, noting that the weld pool was easy to control, produced a thin slag, and required no grinding. FCAW required about 2 hours to complete compared with about 8 hours for SMAW, which was a four-fold improvement in productivity. FCAW also produced clean RT results. The welder also noted that both SMAW fillers performed similarly in terms of weldability, but that the 312 SMAW filler metal was slightly more difficult to weld.

The Radiographic Testing Notes column of Table 9 provides the fabricator's notes from RT of the DMW specimens. Figure 12 shows an example of the RT results for specimen PQR-1 with multiple indications across the weld, representing multiple slag inclusions and porosity. In Figure 12, the A36 steel is on top of the image, and the 50CR steel is on the bottom. The slightly lighter weld metal is faintly visible horizontally across the middle of the image.

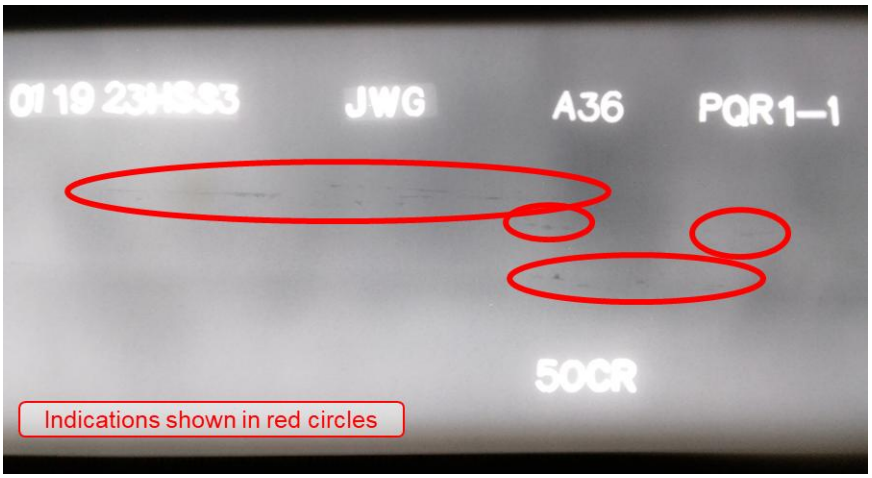

Figure 12. Image from Fabricator Radiographic Testing Results for PQR-1 Specimen Showing Multiple Indications. A36 = A36 steel; 50CR = 50CR steel.

Similarly, Figure 13 shows an example of the RT results for specimen PQR-10. As Table 9 indicates, this specimen had a crack along its entire length when welded. In Figure 13, the 50CR steel is on top of the image, and the 50W steel is on the bottom.

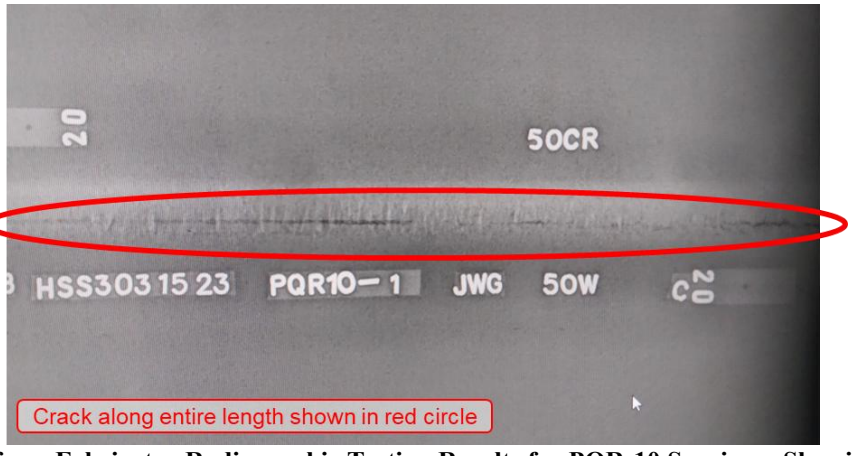

Figure 13. Image from Fabricator Radiographic Testing Results for PQR-10 Specimen Showing Crack along Full Length. 50CR = 50CR steel; 50W = 50W steel.

As Table 9 notes, some of the RT results for the DMW specimens showed “corncob appearances” in the welds. Figure 14 shows an example of this appearance for specimen PQR-15. The corncob appearance is most prevalent near the middle of the image, where the weld resembles kernels on a corncob. This occurrence is problematic because it is difficult to determine whether these appearances are indications in the weld that need to be repaired or they are simply artifacts that appeared during RT. The latter is also problematic because they could mask other indications behind them. In these cases, the welder noted that they did not suspect any indications in these specimens, so they were accepted as-is.

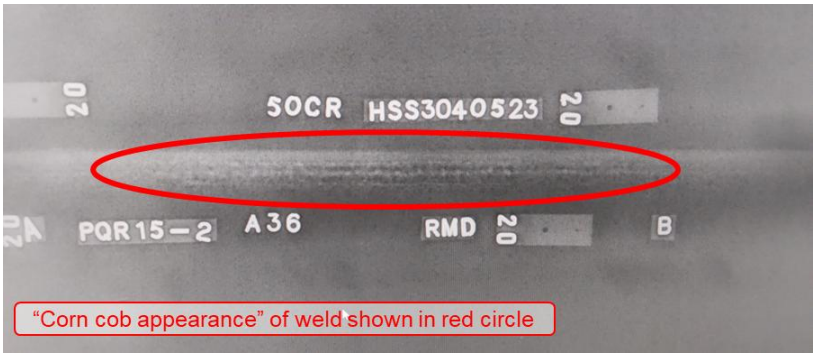

Figure 14. Image from Fabricator Radiographic Testing Results for PQR-15 Specimen Showing “Corncob Appearance” of Weld. A36 = A36 steel; 50CR = 50CR steel.

The welder observed notable distortion in nearly all the Group 1 DMW specimens, including one case in which distortion in a specimen caused the bolts holding the welded plate to pull through the welding table. The welder noted that the Group 2 and 3 specimens were much easier to weld than the Group 1 specimens. The weld beads appeared nice and smooth throughout welding. Welding these specimens was clean and easy, with good fusion to bevel walls. The Group 2 and 3 specimens were also much flatter with minimal distortion.

Weldability and Metallurgical Examination

Metallographic Analysis of Base Metals

The microstructure of the 50CR steel revealed a dual-phase ferritic-martensitic structure, whereas the A36 and 50W steels exhibited a ferritic-pearlitic microstructure (Figure 15).

Macrostructural Analysis of Welds

The macrographs in Figure 16 were captured at low magnification to illustrate the overall weld anatomy, including the base metals, fusion zones, and HAZs. The base metals, labeled as A36, 50CR, and 50W, are the unaffected regions of the original materials on either side of the weld. The fusion zone is the central region of the weld where complete melting and subsequent solidification occurred during welding, resulting in a distinct weld bead structure. HAZs appear as bright bands between the base metals and the fusion zones, representing areas that experienced sufficient thermal exposure to alter their microstructure without reaching the melting point.

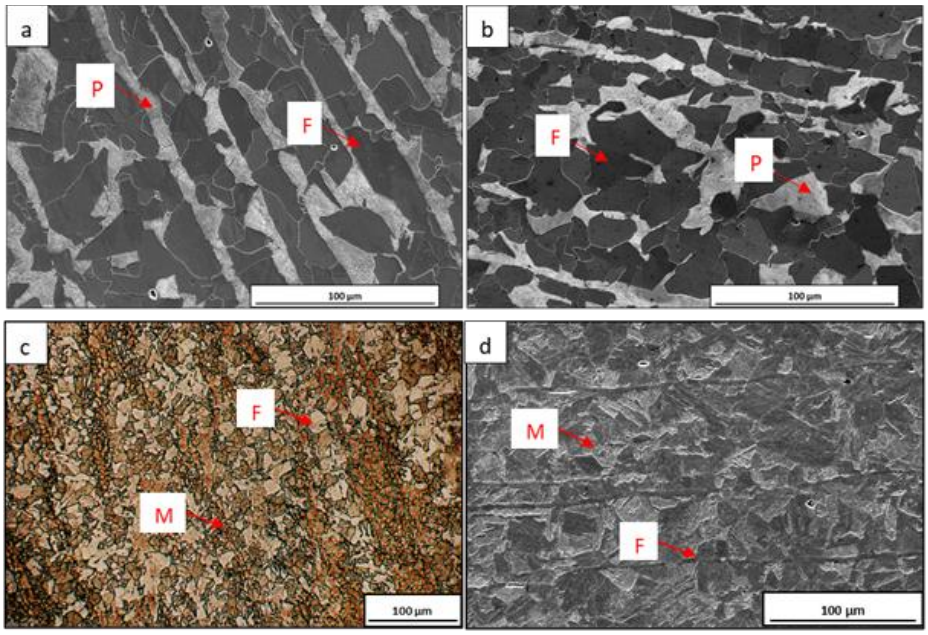

Figure 15. Microstructure of the Base Metals: (a) SE Micrograph of A36 Steel; (b) SE Micrograph of 50W Steel; (c) Optical Micrograph of 50CR Steel; (d) SE Micrograph of 50CR Steel. F = ferrite; M = martensite; P = pearlite; SE = secondary electron.

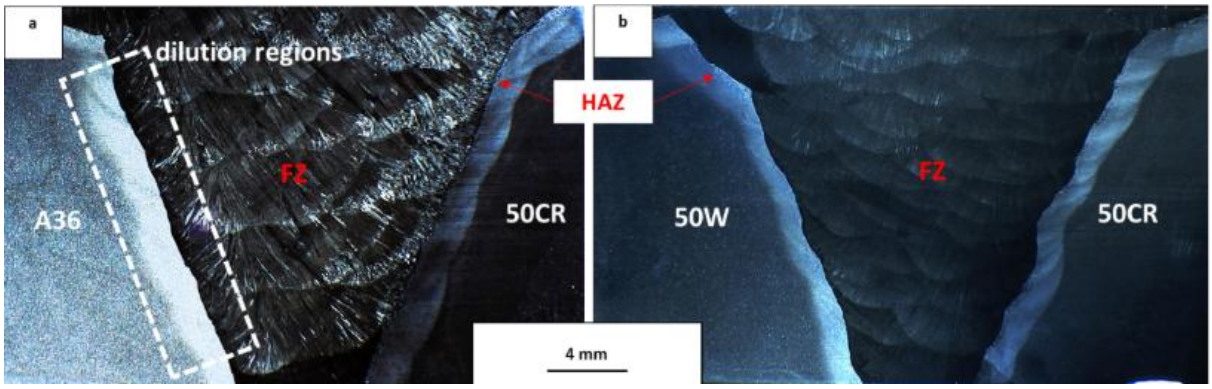

Figure 16. Macro-Etched Weld Profiles of Specimens: (a) PQR-1 and (b) PQR-3, Highlighting the Different Regions of the Weld. 50CR = 50CR steel; 50W = 50W steel; A36 = A36 steel; FZ = fusion zone; HAZ = heat-affected zone.

Note that the dilution regions are also labeled in Figure 16. Dilution is the portion of the base metal that mixes with the weld filler during welding. In the case of these DMWs, dilution refers to the base metals (A36, 50W, 50CR, or 412 steels) melting and mixing with the austenitic stainless steel filler metals. Dilution is typically reported in terms of a ratio of the amount of melted base metal to the total amount of fused metal. For example, a weld with 10% dilution contains 10% base metal and 90% filler metal. The size of the HAZ and dilution for a given welding geometry increased with heat input, aligning with findings from other studies in the literature (Esfahani, 2015). For example, Group 1 welds with typical heat input had dilution values of approximately 20%, whereas Group 1 welds with high heat input had dilution values of approximately 23%.

Solidification Cracking

Significant challenges were encountered in producing successfully welded joints for the Group 1 welds. Among the observed types of cracking, solidification cracking was identified as the most common and severe. Figure 17 shows examples of these cracks observed in the Group 1 DMW specimens.

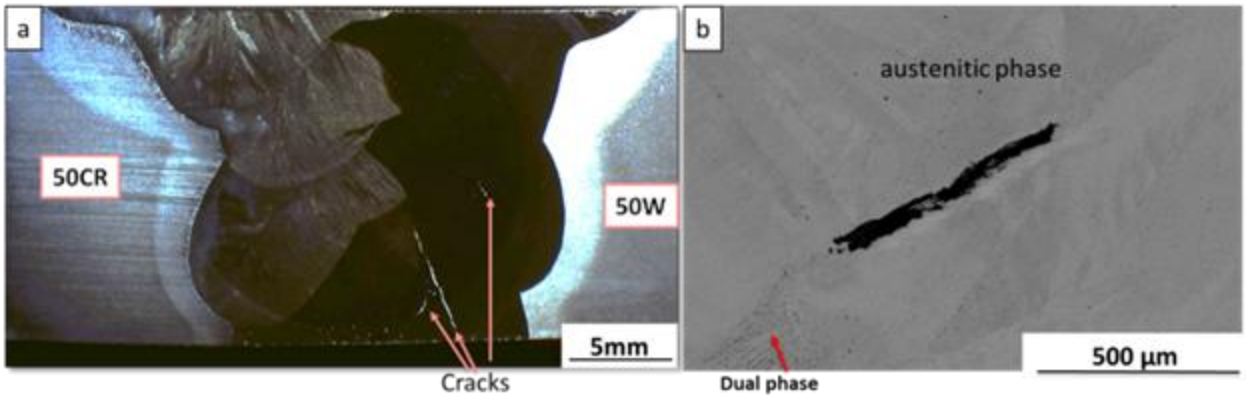

Figure 17. Example of Solidification Cracks in Different Submerged Arc Welding: (a) Extensive Cracking in Specimen PQR-10 with High Heat Input; (b) Micro-Level Cracking in Specimens PQR-13 with Typical Heat Input. 50CR = 50CR steel; 50W = 50W steel.

Once the cracks were observed, the influence of different welding parameters on cracking was evaluated. Samples welded with high heat input (PQR-9 and PQR-10) exhibited significant dilution and severe cracking in the fusion zone, particularly near the carbon steel side. The results revealed a direct correlation between heat input and the severity of solidification cracking. Specifically, welds produced with high heat input exhibited extensive cracking, whereas typical heat input conditions led to significantly shorter cracks (Figure 17).

Although most solidification cracks in the Group 1 welds were observed in specimens using the SAW process, a few microscopic cracks were also detected in Group 1 welds using the SMAW process. Figure 18 shows a macrograph of the SMAW fusion zone, where a single-phase austenitic region had formed in the dilution zone near the carbon steel side. Solidification cracking consistently appeared in this region across multiple samples for Group 1 welds using both SAW and SMAW. It is well established that a small amount of delta ferrite is essential for preventing solidification cracking. However, significant dilution occurred in the fusion zone near the carbon steel side during solidification. This occurrence led to the formation of a fully austenitic region adjacent to the carbon steel plate rather than the necessary delta ferrite. Notably, all solidification cracks observed in the Group 1 DMW specimens were within this single-phase austenitic region.

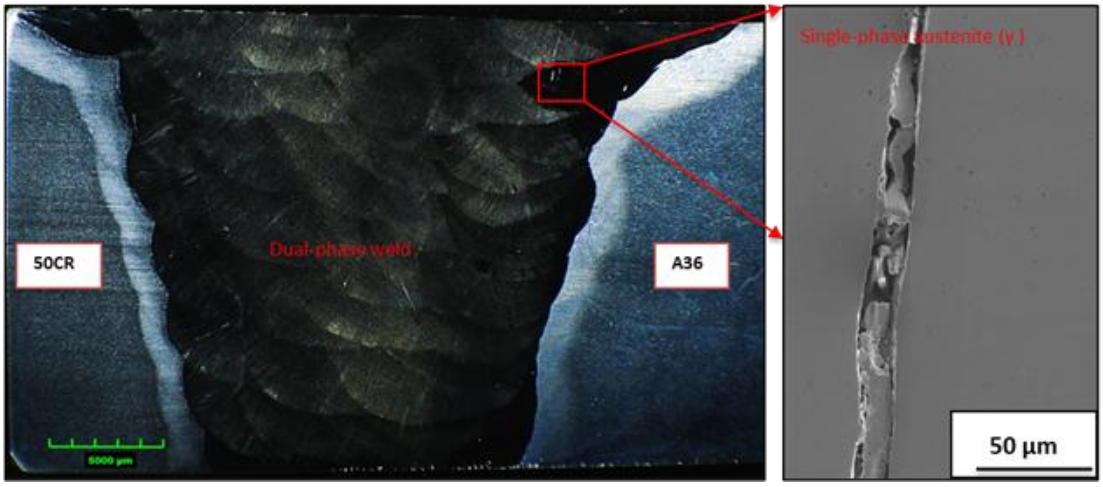

Figure 18. Example of Solidification Cracking in Specimen PQR-2 Using Shielded Metal Arc Welding, where Cracking Occurred within the Single-Phase Austenitic Region. 50CR = 50CR steel; A36 = A36 steel.

The crack tips were further examined using SEM and EDS, and impurities and slag inclusions were found along the edges of the cracks. This analysis revealed that the slag contained high concentrations of impurities, including calcium, silicon, oxygen, and aluminum. Among these elements, silicon has a lower melting point than the 309L weld metal, meaning it will segregate toward the centerline of the weld and will be the last portion of the weld to solidify, as Figure 11 illustrated previously.

The discovery of these cracks prompted changes to be made to the welding parameters used for the Group 2 and 3 welds. The two changes involved both the heat input and the weld joint geometry to mitigate the cracking susceptibility. For the Group 2 SAW specimens, the heat input was reduced to approximately 31.5 kJ/in, down from approximately 36 to 43 kJ/in for the typical heat input and approximately 60 kJ/in for the high heat input specimens from the Group 1 welds. As part of this decrease in heat input, the welding speed was increased to 20 inches per minute. Increasing the welding speed helped mitigate solidification cracking by enhancing the cooling rate during solidification.

For the Group 2 and 3 welds, the weld joint geometry was also changed to a single-V with backgouge. Previously, all Group 1 welds used a single-V geometry with carbon steel backing. The single-V with backgouge produces similar geometry to double-V joints. Double V-groove joints in welding typically provide substantial benefits over single-V joints by effectively reducing welding-induced deformation and the resulting transverse internal and residual stresses (Taraphdar et al., 2021; Vamsi Krishna et al., 2024; Zhang and Tian, 2022). The single-V with backgouge joint also eliminated the need for the carbon steel backing bar, which removed another source of solidification cooling and the potential for impurities from the carbon steel backing bar to migrate into the weld metal during dilution.

Based on this analysis, the fabricator welded the Group 2 and 3 DMW specimens by using a low-heat input and a single-V with backgouge joint. These welds were then examined using optical microscopy and SEM, and no cracks were found in any of these specimens. This

examination showed that the modifications to the welding processes alleviated the solidification cracking and can serve as guidelines for producing defect-free welds in similar DMWs.

Cold Cracking

In addition to the solidification cracks, a second type of crack was identified in specimens PQR-13 and PQR-14 at the root pass, where the weld metal was deposited directly onto the carbon steel backing plate. These two specimens were Group 1 welds made with the SAW process using a typical heat input and a 309L filler. This type of cracking often develops after cooling and is influenced by joint constraint, cooling rate, and hardness of the welded region. Direct contact between the filler metal and the carbon steel backing plate allowed significant mixing between the filler metal and the backing plate, leading to substantial dilution of chromium and nickel in the fusion zone. In addition, the carbon steel backing plate acted as a heat sink, accelerating the cooling rate of the weld.

The fusion zones of specimens with cold cracking were examined under an SEM for further analysis. The microstructure of the root weld passes directly adjacent to the carbon steel, where the cracks were observed, predominantly consisting of martensite with some retained austenite. This microstructure was distinctly different from the surrounding weld passes and upper regions of the fusion zone, indicating that a phase transformation had occurred in the cracked zone.

Vickers hardness measurements were taken at various locations across these welds. Figure 19 shows an example of these hardness measurements, with Figure 19a showing a composite SEM micrograph of the weld with hardness traverse measurement locations and Figure 19b showing the hardness results.

As Figure 19 shows, the root pass of the weld (where the cracks were observed) had much greater hardness values compared with the top or middle of the weld. This observation suggested that the microstructure of this portion of the weld was brittle martensite. The presence of residual welding stresses, combined with the formation of brittle martensite in the root pass, is believed to have caused the cold cracking. The cold cracking was resolved in the Group 2 and 3 welds because of the use of the single-V with backgouge weld joint geometry. This joint type eliminated the need for carbon steel backing plates and mitigated the risk of dilution-induced cold cracking. No cold cracks were found in any of the Group 2 and 3 welds.

The presence of residual welding stresses, combined with the formation of brittle martensite in the root pass, is believed to have caused the cold cracking. The cold cracking was resolved in the Group 2 and 3 welds by using the single-V with backgouge weld joint geometry. This joint type eliminated the need for carbon steel backing plates and mitigated the risk of dilution-induced cold cracking. No cold cracks were found in any of the Group 2 and 3 welds.

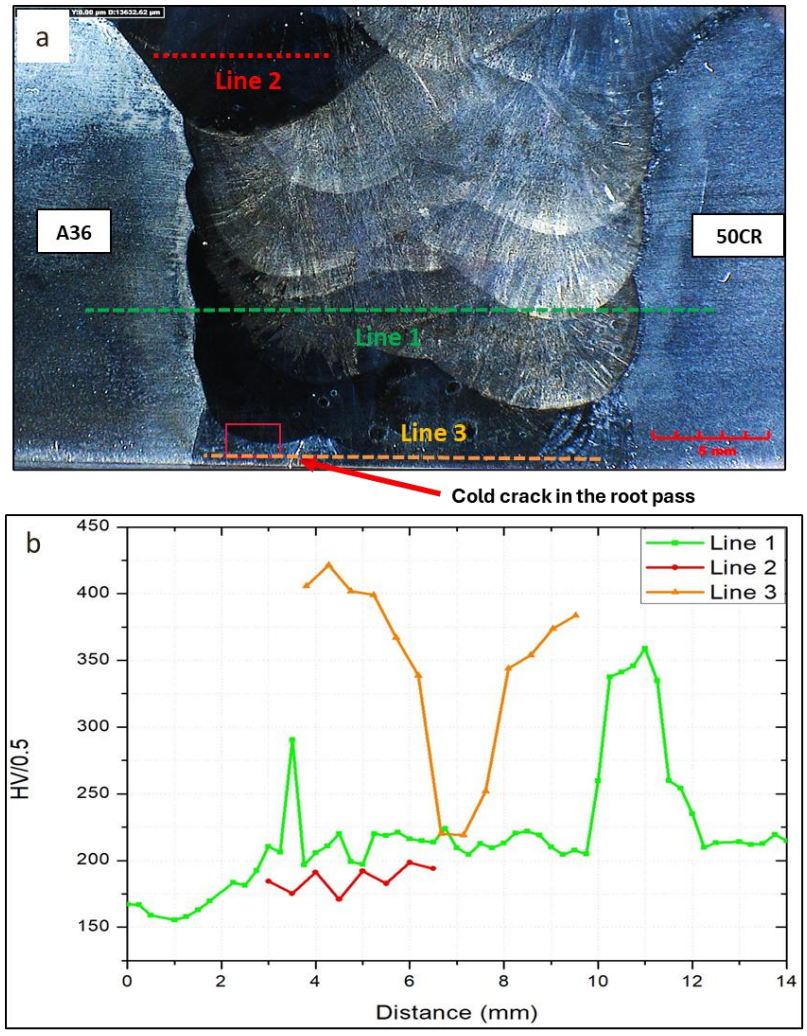

Figure 19. Overview of Cold Cracking Analysis: (a) Macroscopic View of Specimen PQR-13 with Root Pass Crack; (b) Vickers Hardness Profile across Weld Regions with Hardness Lines Indicated in the Macrograph. A36 = A36 steel; 50CR = 50CR steel.

Summary of Weldability and Metallurgical Examination

As expected, the 50CR steel and the two carbon steels (A36 and 50W) exhibited different base metal microstructures and chemical compositions. Significant dilution, or mixing of the filler metal and base metal, occurred on both sides of the welds during welding the DMW specimens. The dilution was found to be a function of the heat input during welding. For Group 1 welds, dilution from the carbon steel side of the weld introduced impurities such as sulfur into the weld metal, causing solidification cracking. The Group 1 welds also experienced cold cracking because of dilution and the accelerated cooling rate from the carbon steel backing. All forms of cracking were alleviated in the Group 2 and 3 welds by reducing the heat input and using a single-V with backgouge weld joint.

Mechanical Testing

Table 10 shows a summary of the mechanical testing results compared with their respective specified pass-fail requirements. The following sections discuss additional details about the results of each test type.

Table 10. Pass-Fail Summary of Mechanical Test Results

Group Number	Specimen Name	Side-Bend Testing	Reduced Section Tension Testing	All Weld-Metal Testing	Charpy V-Notch Testing[a]
1	PQR-1	Pass	Pass	Pass	Pass
1	PQR-2	Pass	Pass	Pass	Pass
1	PQR-3	Pass	Fail	Pass	Pass
1	PQR-4	Pass	Pass	Pass	Pass
1	PQR-9	Fail			
1	PQR-10	Fail			
1	PQR-13	Fail	Pass	Pass	Pass
1	PQR-14	Fail	Pass	Pass	Pass
1	PQR-15	Fail			
1	PQR-16	Fail			
2	PQR-17	Pass	Pass	Pass	Pass
2	PQR-18	Pass	Pass	Pass	Pass
2	PQR-19	Pass	Pass	Pass	Pass
2	PQR-20	Pass	Pass	Pass	Pass
3	PQR-21	Pass	Pass	Pass	Pass
3	PQR-22	Pass	Pass	Pass	Pass
3	PQR-23	Pass	Pass	Pass	Pass
3	PQR-24	Pass	Pass	Pass	Pass
3	PQR-25	Fail	Pass	Pass	Pass
3	PQR-26	Fail	Pass	Pass	Pass
3	PQR-27	Pass	Pass	Pass	Pass
3	PQR-28	Pass	Pass	Pass	Pass

AASHTO = Association of State Highway and Transportation Officials; AWS = American Welding Society; PQR = procedure qualification record. [a] The Charpy V-Notch tests for Group 1 and 2 specimens were conducted at 40ºF, so they were compared with the fracture critical requirements for ASTM A709 Grade 50CR steel. Tests for the Group 3 specimens were conducted at 0ºF, so they were compared with the fracture critical requirements for Grade 50CR steel in the AASHTO Temperature Zone II in AASHTO/AWS D1.5.

Side-Bend Testing

The side-bend tests were the first type of mechanical test conducted on the DMW specimens because the tests were easy to conduct, and they represent a severe loading condition on the welded samples. Therefore, they served as a good initial evaluation.

As Table 10 shows, of the Group 1 specimens, only SMAW and FCAW specimens (PQR-1 through PQR-4) passed the side-bend tests, whereas all the SAW specimens (PQR-9

through PQR-16) failed. Among the SAW specimens, those using “typical” heat input values (PQR-13 through PQR-16) had much smaller cracks compared with specimens that had “high” heat input values (PQR-9 and PQR-10). In fact, many of the specimens with “high” heat input values broke completely in half during side-bend testing. Figure 20 shows example photos from each of these two heat input conditions.

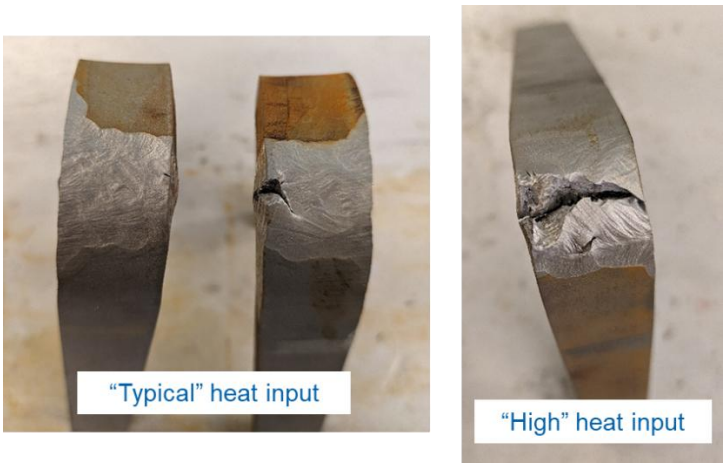

Figure 20. Example Photos of Side-Bend Tests of Specimens with Typical and High Heat Input

These results suggested that heat input plays a critical role in the weldability of DMWs. More specifically, smaller heat input values produced better weldability. These results also suggested that SAW may be more difficult to create structurally sound DMWs compared with SMAW and FCAW. This outcome was due to the greater heat input used during the SAW process compared with SMAW and FCAW (see actual heat input values used for the welds in Table 9). These results agreed with the results from the weldability and metallurgical examinations and therefore led to reduced heat input for the Group 2 and 3 specimens.

Table 10 shows that all the Group 2 specimens, which were all SAW welds, passed the side-bend testing requirements. This result showed that smaller heat inputs helped to solve the cracking challenges observed in the side-bend testing of the Group 1 specimens.

Of the Group 3 specimens using 412 steel, all the FCAW specimens (PQR-21 through PQR-24) passed the side-bend tests. Of the Group 3 SAW specimens, only those specimens using the 309L solid filler (PQR-25 and PQR-26) failed the side-bend tests. The other Group 3 SAW specimens used the 309L cored filler. This scenario again suggests that SAW may be more difficult to use to create structurally sound DMWs compared with FCAW. However, this difficulty can be overcome by using the 309L cored filler, which results in a microstructure that is more resistant to cracking compared with the 309L solid filler (Fitz-Gerald et al., 2020).

Reduced Section Tension Testing

Figure 21 shows the average results from the reduced section tension testing. All the test results passed the minimum tensile strength requirement. For DMW specimens made with A36 steel, this requirement was 58 ksi, and for DMW specimens made with 50W steel, it was 70 ksi. All the samples failed in ductile behavior in the carbon steel base metal, except for one of the

PQR-3 test samples. These samples failed prematurely in the HAZ of the A36 steel side at a strength below the required limit. Therefore, PQR-3 was deemed to have failed the reduced section tension testing.

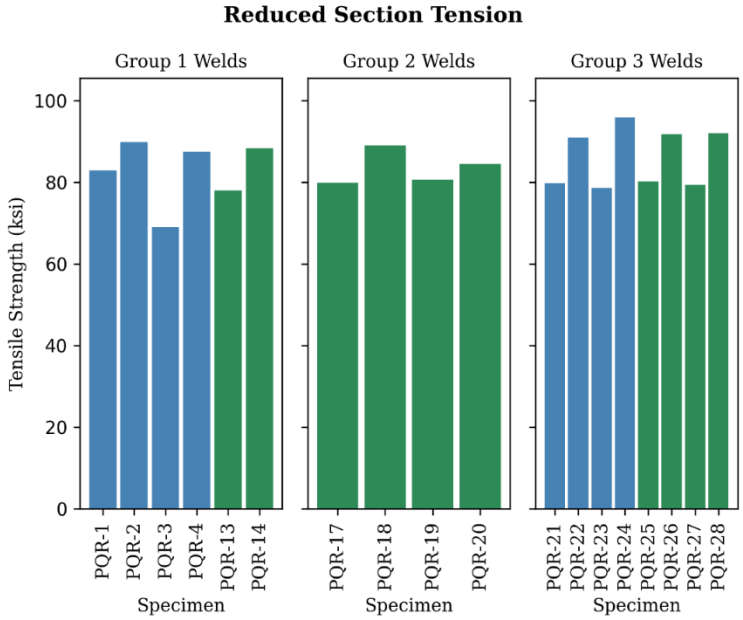

Figure 21. Average Reduced Section Tension Testing Results. Blue bars represent shielded metal arc welding or flux cored arc welding, and green bars represent submerged arc welding.

Note in Figure 21 that for sequential pairs of DMW specimens, such as PQR-1 and PQR-2 or PQR-25 and PQR-26, the first specimen of the pair has a smaller tensile strength and the second of the pair has a greater tensile strength. This occurrence was due to the first specimen of the pair having a lower strength A36 steel base metal, whereas the second specimen of the pair had a higher strength 50W steel base metal. Overall, only slight differences were found in the tensile strengths of the reduced section tensile tests between DMW specimens of different weld groups.

All Weld-Metal Tension Testing

The all weld-metal tension testing consisted of analyzing data for the yield strength, tensile strength, and elongation of the test specimens. Figure 22 shows the average results for the yield strength of the all weld-metal tension testing. All the test results passed the minimum yield strength requirement. For DMW specimens made with A36 steel, this requirement was 45 ksi, and for DMW specimens made with 50W steel, it was 50 ksi.

In Figure 22, PQR-3 and PQR-4 had much greater yield strengths than PQR-1 and PQR-2. Similar trends are present when comparing PQR-23 and PQR-24 to PQR-21 and PQR-22. Of these specimens, those with greater yield strengths were all welded using the 312 filler metal. Therefore, the 312 filler metal can produce greater yield strengths compared with the 309L filler for the SMAW and FCAW processes.

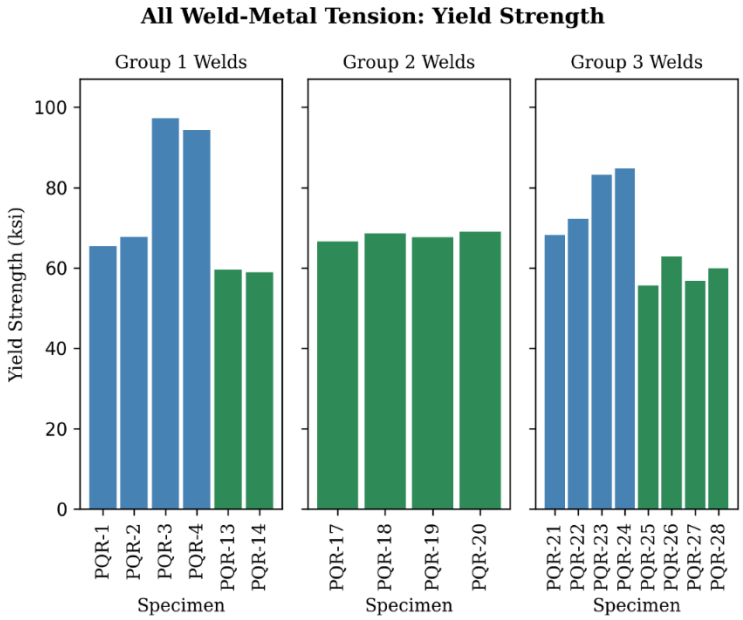

Figure 22. Average Results for Yield Strength of All Weld-Metal Tension Testing. Blue bars represent shielded metal arc welding or flux cored arc welding, and green bars represent submerged arc welding.

Figure 23 shows the average results for the tensile strength of the all weld-metal tension testing. All the test results passed their minimum tensile strength requirements. For DMW specimens made with A36 steel, this requirement was 60 ksi, and for DMW specimens made with 50W steel, it was 65 ksi. Figure 23 shows similar trends to those observed for the all weld-metal yield strength results.

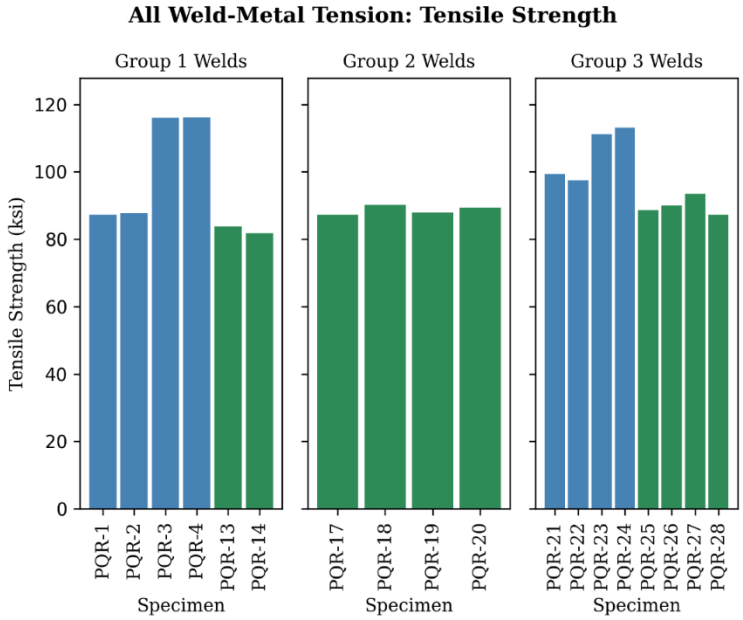

Figure 23. Average Results for Tensile Strength of All Weld-Metal Tension Testing. Blue bars represent shielded metal arc welding or flux cored arc welding, and green bars represent submerged arc welding.

Figure 24 shows the average results for the elongation of the all weld-metal tension testing. All test results passed the minimum elongation requirement of 22% for both A36 and 50W steel. From Figure 24, the DMW specimens made using the 312 filler (PQR-3, PQR-4, PQR-21, and PQR-22) had lower elongation values than the other SMAW and FCAW specimens made using the 309L filler. This scenario illustrates that although the 312 filler provides an increase in yield and tensile strengths, it also provides a decrease in elongation. This observation was much less pronounced in the Group 3 specimens than in the Group 1 specimens. This result could have been due to a lower heat input during welding for the Group 3 specimens.

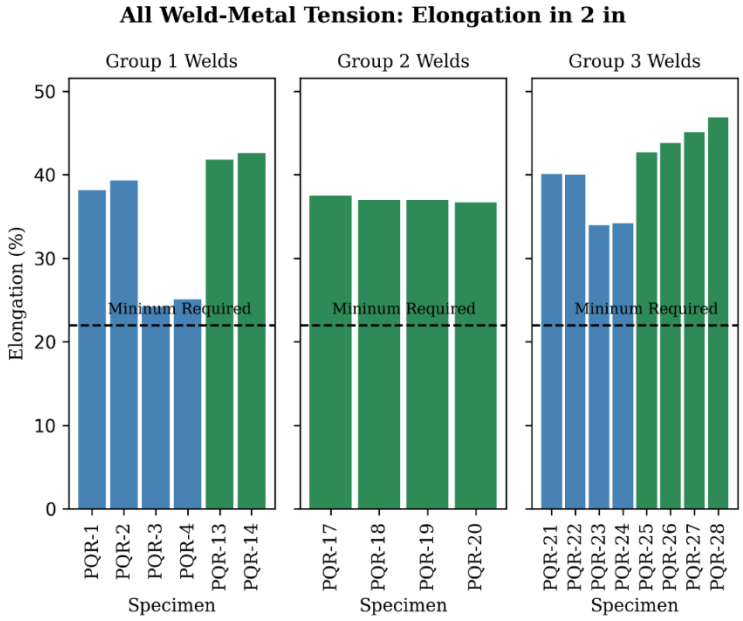

Figure 24. Average Results for Elongation of All Weld-Metal Tension Testing. Blue bars represent shielded metal arc welding or flux cored arc welding, and green bars represent submerged arc welding.

Charpy V-Notch Testing

Figure 25 shows the results for the CVN testing. The Group 1 and 2 specimens were tested at 40ºF in error, rather than the intended test temperature of 0ºF, which is the AASHTO Temperature Zone II (where Virginia is located) in D1.5. Therefore, the Group 1 and 2 specimens were compared with the fracture critical requirements in ASTM A709, which requires 25 ft-lbs. when tested at 40ºF (ASTM International, 2021b). The Group 3 welds were compared with the requirements in D1.5 for AASHTO Temperature Zone II, which requires 20 ft-lbs. when tested at 0ºF. Figure 25 shows both minimum requirements (AASHTO and AWS, 2020).

As the Group 1 welds show in Figure 25, the average PQR-4 results failed to meet the minimum CVN requirement for fracture critical members according to ASTM A709 when tested at 40ºF. PQR-3 passed these requirements but had CVN values much less than many of the other specimens. Both PQR-3 and PQR-4 used 312 filler. When combined with the other mechanical testing results, the Group 1 specimens with 312 filler exhibited greater strength but lower ductility and fracture toughness values. However, the Group 3 specimens PQR-23 and PQR-24 also used 312 filler. These specimens produced CVN values that were similar to the values of the other FCAW specimens in this group. Therefore, when used with smaller heat input values,

specimens with 312 filler produced passing results. This outcome is another benefit of using smaller heat inputs with these DMWs.

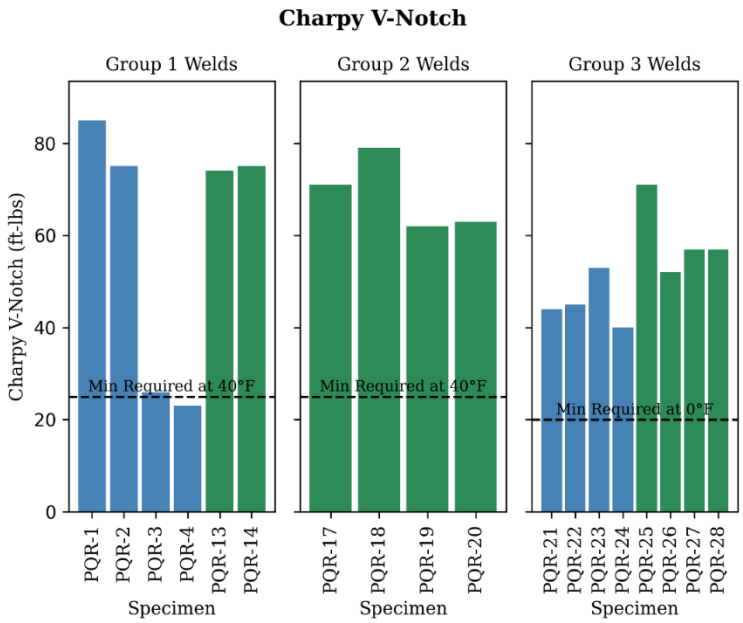

Figure 25. Average Results for Charpy V-Notch Testing. Blue bars represent shielded metal arc welding or flux cored arc welding, and green bars represent submerged arc welding.

Mechanical Testing Summary

Overall, the mechanical test results showed that the side bend tests produced a severe loading condition and were effective at screening the mechanical properties of the DMWs. All the Group 1 welds using SAW failed the side bends. However, nearly all the Group 2 and Group 3 welds using the lower heat input and single-V with backgouge passed all the mechanical testing requirements. With the Group 1 welds, specimens using 312 filler produced greater yield strengths but lesser ductility and CVN results. This trend was less apparent in the Group 2 and 3 welds, which used the lower heat input and single-V with backgouge weld joint geometry. For DMWs made using 412 steel, all the FCAW specimens passed the mechanical test requirements. However, for the SAW specimens, only those specimens using the 309L cored filler passed the requirements.

Corrosion Testing

Saltwater Droplet Testing

Figure 26 shows the average pitting depth measurements of DMW specimens PQR-17 through PQR-20 after saltwater droplet testing. Note that PQR-17 and PQR-19 used A36 steel for their carbon steel base metal, whereas PQR-18 and PQR-20 used 50W steel. In Figure 26, lines of different colors represent the different specimens, as the legend shows, and the points represent the average value from all the pitting measurements. Pitting depth measurements from

all three bulk material locations were combined because no observable differences between these locations were found.

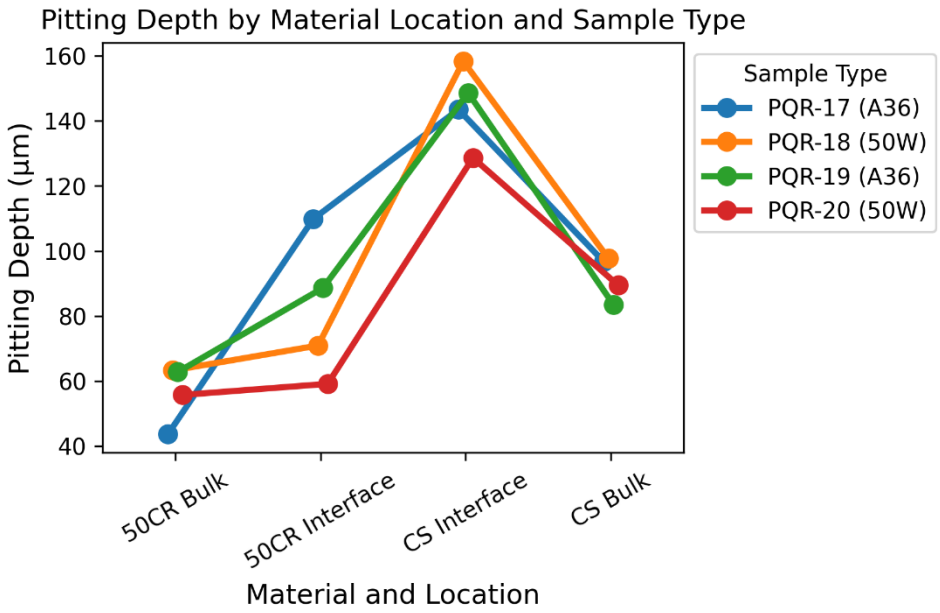

Figure 26. Plot Showing Average Pitting Depth Measurements for Dissimilar Metal Weld Samples Exposed to Saltwater Droplet Testing. 50 CR = 50CR steel; 50W = 50W steel; A36 = A36 steel; CS = carbon steel.

Some trends can be observed by pitting depth measurements of the bulk material versus material at the weld interface. For example, the average pitting depth measurements for all four specimens at the 50CR steel bulk material were approximately 40 to 60 µm. At the 50CR steel weld interface, the average pitting depth of all the specimens increased to approximately 60 to 110 µm. In fact, the pitting depth for all four specimens increased when comparing results at the 50CR steel interface to the 50CR steel bulk material.

The same trend is true when examining the pitting depth results on the carbon steel side of the welds. For example, average pitting depth measurements at the carbon steel bulk location for all four specimens ranged from about 80 to 100 µm. At the carbon steel weld interface, the average pitting depth was approximately 130 to 160 µm. This scenario again shows an increase in the average pitting depth in the base metal at the weld interface compared with the bulk material. These trends suggest that galvanic corrosion is contributing to this increase in pitting depth.

Width-to-depth ratios for the pits in all the specimens were also calculated to determine whether galvanic corrosion influenced them. These ratios were calculated because of the difference in pit formation in stainless steel versus carbon steel. In general, stainless steels, like 50CR steel or austenitic stainless steel, tend to exhibit more localized corrosion with fewer pits that are narrower and deeper, whereas carbon steels, like A36 or 50W, tend to exhibit more uniform corrosion with wider and shallower pits. The pitting width-to-depth ratio was especially of interest because pits with smaller width-to-depth ratios have the potential to be more crack-like and could lead to other failure mechanisms, such as fatigue or fracture.

Figure 27, which is similar to Figure 26, shows the average pit width-to-depth ratios for specimens PQR-17 through PQR-20. When looking at the 50CR steel side of the welds, the pit width-to-depth ratio appeared to remain relatively similar when comparing the 50CR interface versus the 50CR bulk locations. This scenario suggests that galvanic corrosion did not alter the pit width-to-depth ratio on the 50CR steel side of the weld. However, for the carbon steel side of the weld, the pit width-to-depth ratio is smaller at the carbon steel interface compared with the carbon steel bulk material for all four specimens tested. This outcome means that pits at the carbon steel weld interface were narrower and deeper than the pits in the carbon steel bulk material.

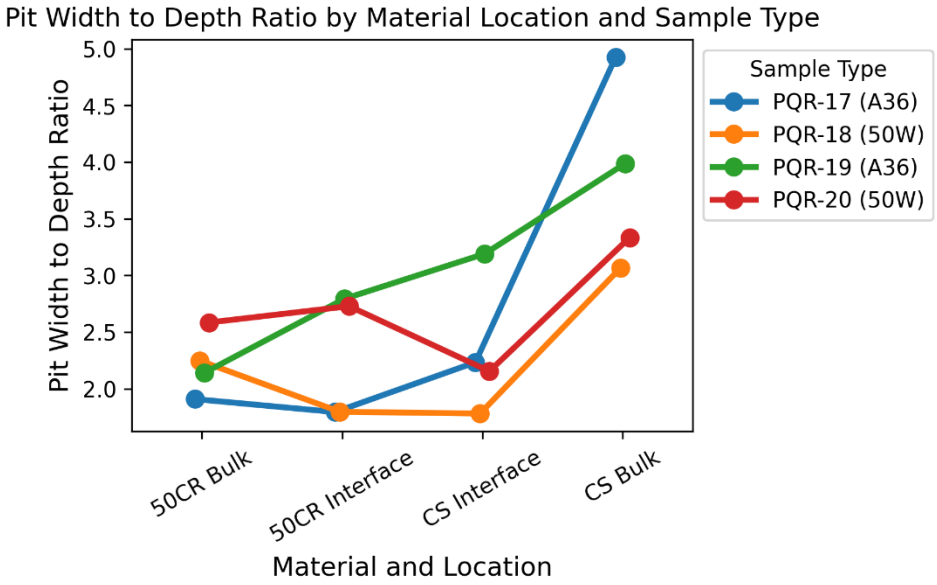

Figure 27. Plot Showing Average Pitting Width to Depth Ratio for Dissimilar Metal Weld Samples Exposed to Saltwater Droplet Testing. A36 = A36 steel; 50CR = 50CR steel; 50W = 50W steel; CS = carbon steel.

Although the pit width-to-depth ratio at the carbon steel weld interface was found to be smaller than that in the carbon steel bulk material because of galvanic corrosion, the value of the ratios does not suggest that these pits are crack-like. This finding can be observed by the pit width-to-depth ratio values in Figure 27. The average ratios at the carbon steel weld interface range from approximately 1.8 to 3.2. These ratios are similar to the ratios found at the 50CR steel bulk material and the 50CR weld interface. For this reason, these narrower and deeper pits at the carbon steel weld interface are not expected to cause cracking issues.

Accelerated Corrosion Chamber Testing

Figure 28 shows close-up photos of typical base metal specimens after the accelerated corrosion chamber testing was completed. The A36 and 50W steels appeared similar, with both exhibiting laminar corrosion with thin sheets of steel separating from the bulk base metal. On the other hand, the 50CR steel appeared to exhibit much smaller corrosion flakes from all over the bulk base metal.

Figure 28. Close-up Photos of Typical Base Metal Specimens before Blast Cleaning for Accelerated Corrosion Chamber Testing

Figure 29 shows close-up photos of typical base metal specimens after blast cleaning. The 50W steel appeared to exhibit more pitting than the A36 steel, with small corrosion pits distributed along its entire surface. In the blast cleaned condition, the 50CR steel appeared to have fewer but deeper pits compared with the 50W steel.

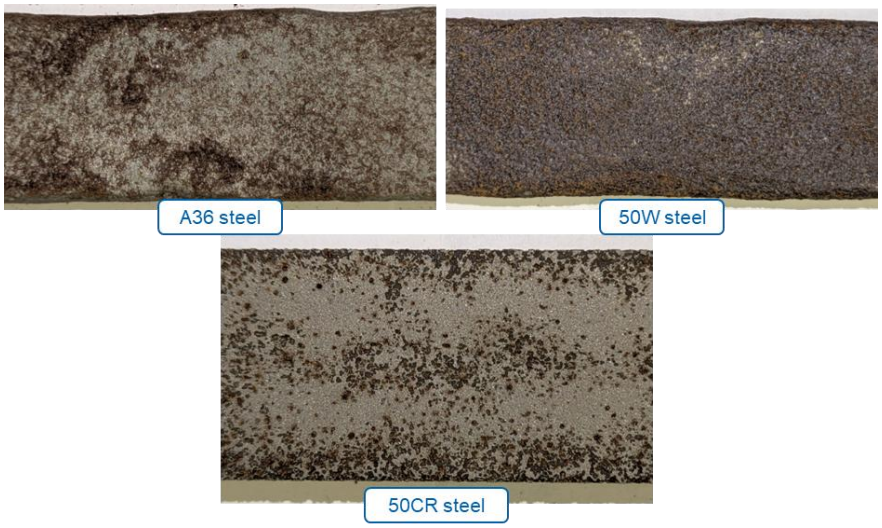

Figure 29. Close-up Photos of Typical Base Metal Specimens after Blast Cleaning for Accelerated Corrosion Chamber Testing

Figure 30 shows close-up photos of the welds from three DMW specimens after blast cleaning. Figure 30 includes one typical specimen from each group: PQR-2 from Group 1, PQR-19 from Group 2, and PQR-23 from Group 3. The general corrosion behavior of each of the

specimens was relatively similar. The carbon steel side of the weld showed heavy thinning directly adjacent to the weld. Farther away from the weld, the carbon steel still corroded but not as severely as in the material directly adjacent to the weld. Galvanic corrosion caused the heavy thinning closer to the weld metal because of the less noble carbon steel being directly connected to the more noble stainless steel weld metal.

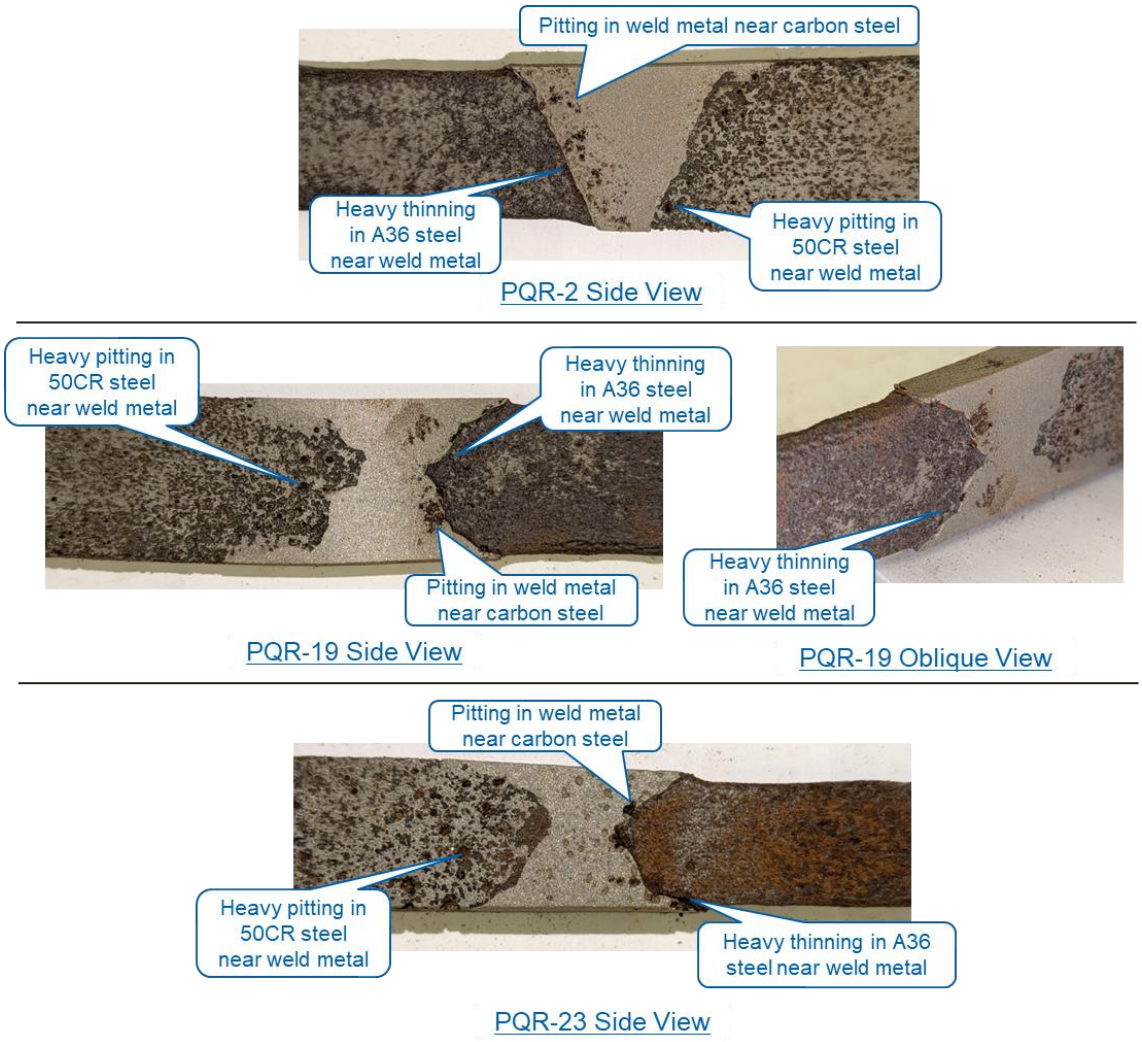

Figure 30. Close-up Photos of Welds of Typical Dissimilar Metal Weld Specimens after Blast Cleaning for Accelerated Corrosion Chamber Testing

The stainless steel weld metal experienced some pitting directly adjacent to the carbon steel base metal but otherwise showed little to no corrosion damage. Pitting was present in the weld metal near the carbon steel base metal because of the dilution that occurred during welding. This dilution caused the carbon steel base metal to mix with the stainless steel filler metal, thereby creating a mixture of the two metal types. In this mixed metal environment, the carbon steel preferentially corroded at a faster rate than the stainless steel, leaving pits in the weld metal adjacent to the carbon steel.

The 50CR steel side of the weld displayed a greater concentration of pits and, in some cases, deeper pits adjacent to the weld compared with the rest of the 50CR steel base metal. As

with the carbon steel, galvanic corrosion caused the heavier pitting directly adjacent to the weld. This heavier pitting was limited to approximately 1/2 inch or less away from the weld fusion line.

Visual Analysis of Partial Immersion and Electrochemistry Testing

Partial immersion testing demonstrated the clear effects of the galvanic couple between the 309L weld metal and the carbon steel, with rust forming across the A36 steel. A film of black-colored corrosion product was also present throughout the entire sample. SEM evaluation along the waterline also showed a large degree of selective attack, which was expected because of the galvanic couple and the poor corrosion resistance of the uncoated carbon steel when exposed to saltwater. Figure 31 shows photographs of a half-immersed weld cross section with galvanic corrosion occurring between the base metals and weld metal.

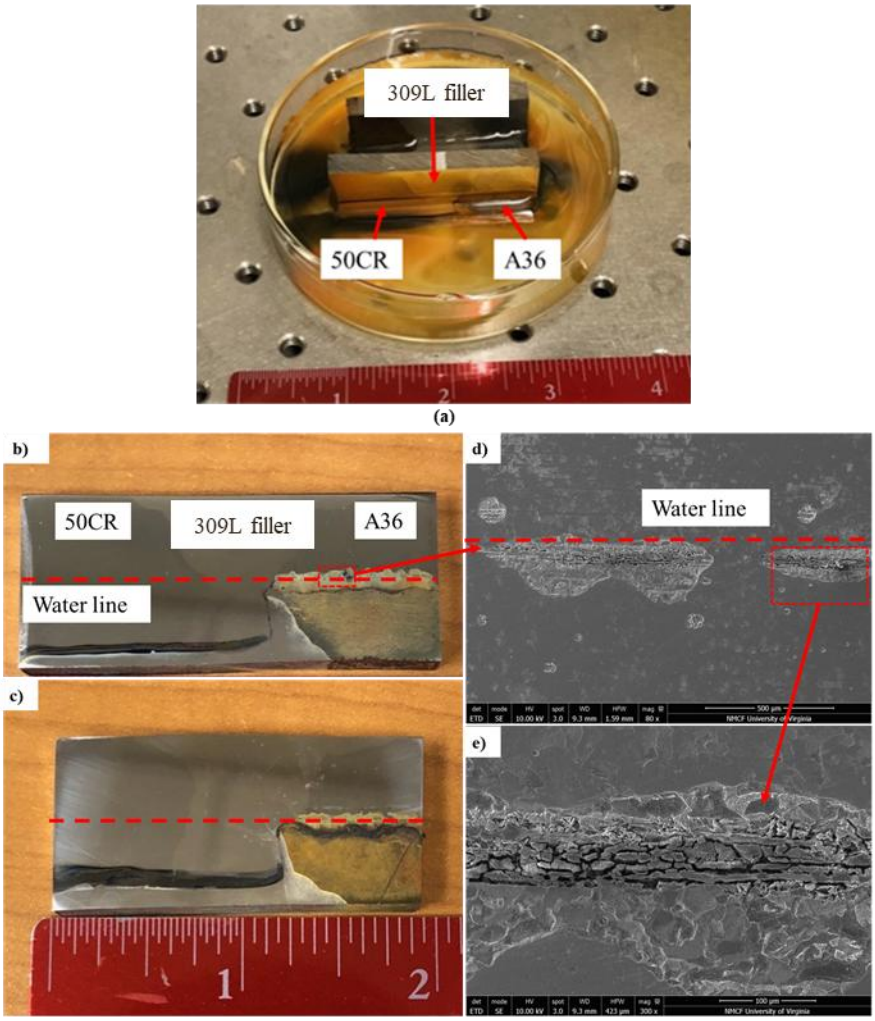

Figure 31. (a) Photograph of a Half-Immersed Weld Cross Section Showing Galvanic Corrosion Occurring between the Weld Metals. This photograph was taken 20 hours after placing the weld into the solution. Photographs of weld cross sections (b) after 20 hours and (c) after 1 week of half immersion. Scanning electron microscopy insets in (d) and (e) show the severe corrosion that occurs along the water-air interface in the meniscus region.

Visual evaluation of the electrochemistry test samples showed similar results. After OCP tests, the 50CR steel and the 309L weld metal both appeared unaffected after 2 or 5 hours. The A36 and 50W steels developed surface corrosion, with visible surface iron oxides (i.e., rust) forming during immersion. After OCP and potentiodynamic scans, the samples were examined using SEM. Results found that both A36 and 50W carbon steels exhibited typical uniform corrosion, 50CR steel showed localized corrosion around impurities, and the 309L weld metal appeared uncorroded. Figure 32 shows optical micrographs of the polarized A36 and 50CR steels. As with OCP testing, the A36 steel showed uniform corrosion, whereas the 50CR steel began to form pits when a potential was applied and clearly exhibited crevicing along the edge of the electrochemical masking tape.

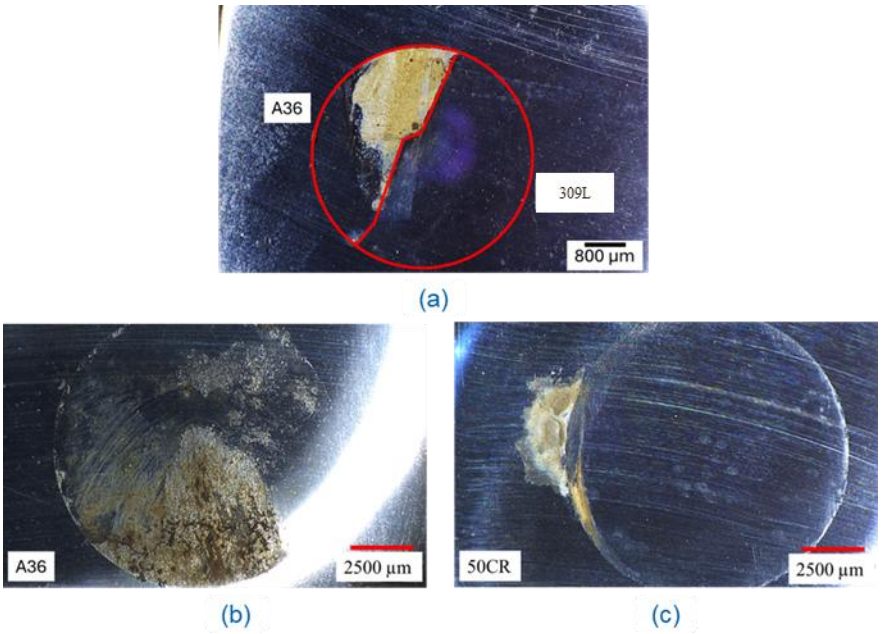

Figure 32. Optical Micrographs Showing the Appearance of Each of the Weld Metal Surfaces after Open Circuit Potential Testing. (a) The A36/309L weld interface after 5 hours of exposure with no polarization, no voltage applied during the monitoring of the weld metal's potential during open circuit potential testing. Red circles denote the areas on the samples that were exposed to the 3.5 wt.% sodium chloride solution. Additional optical micrographs showing the appearance of each of the weld metal surfaces after potentiodynamic testing, so voltage was applied in a controlled manner to encourage corrosion reaction. (b) The A36 steel sample exhibits corrosion, whereas the (c) 50CR steel sample shows corrosion only along the edge of the marked-off area, a crevice, so the general surface area of the 50CR steel was more corrosion resistant than the A36 steel sample when subjected to the same voltage conditions in the same environment.

Electrochemistry Testing: Open Circuit Potential Measurements

Figure 33 shows the OCP testing results. These results provide insight into where corrosion is most likely to occur. In Figure 33, the most noble metal is the cathode, and the most active metal is the anode. The 309L weld metal is the most noble with the most positive OCP value, followed by the 50CR/309L HAZ, 50CR steel, A36/309L HAZ, A36 steel, 50W/309L HAZ, and 50W steel.

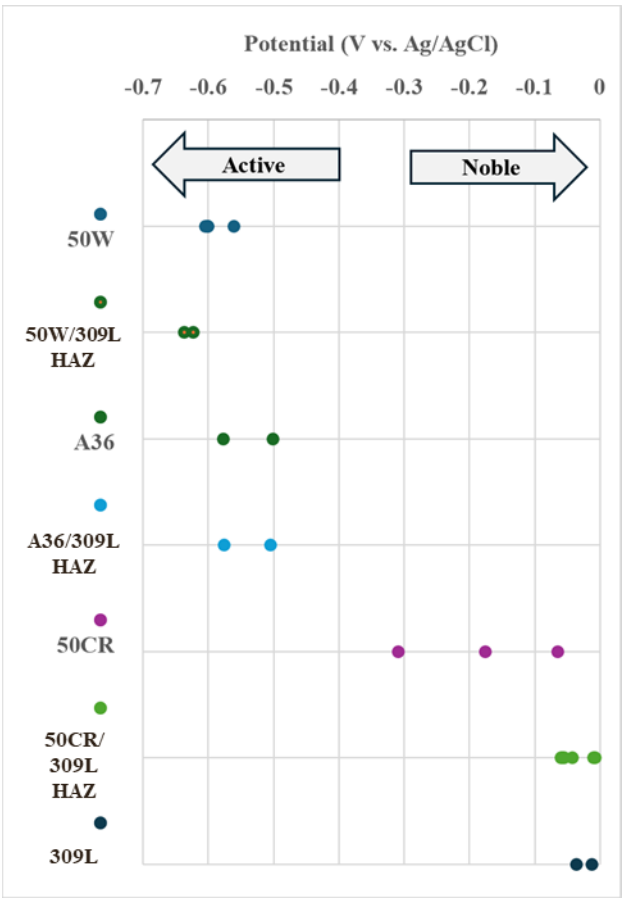

Figure 33. Open Circuit Potential Tests Run for 7,200 Seconds (2 hours) Showing the Relative Nobilities of Each of the Weld Metals Tested in 3.5 wt.% Sodium Chloride Solution. 50CR = 50CR steel; 50W = 50W steel; A36 = A36 steel; HAZ = heat-affected zone.

Electrochemistry Testing: Anodic Polarization Measurements

Anodic polarization scans were performed to assess the pitting potential and susceptibility of each weld metal. Figure 34 shows the anodic polarization results, and the trend in corrosion resistance between each metal was apparent. The 309L weld metal was the most corrosion resistant with a pitting potential of 0.9V, whereas the interface between the 50CR steel and 309L weld metal began to pit as low as 0.15V. Furthermore, after pits increased in size, they reached a much higher current density compared with the 309L weld metal (100 mA/cm^2 versus 100 uA/cm^2, respectively). The 50W steel was a much more active metal, and the 50W steel/309L weld metal interface reached 100 mA/cm^2 at a lower voltage of 0.1V compared with the 50CR steel/309L weld metal. This trend has also been observed for similar types of steels in a 3% NaCl solution at 30ºC (Szklarska-Smialowska, 2005).

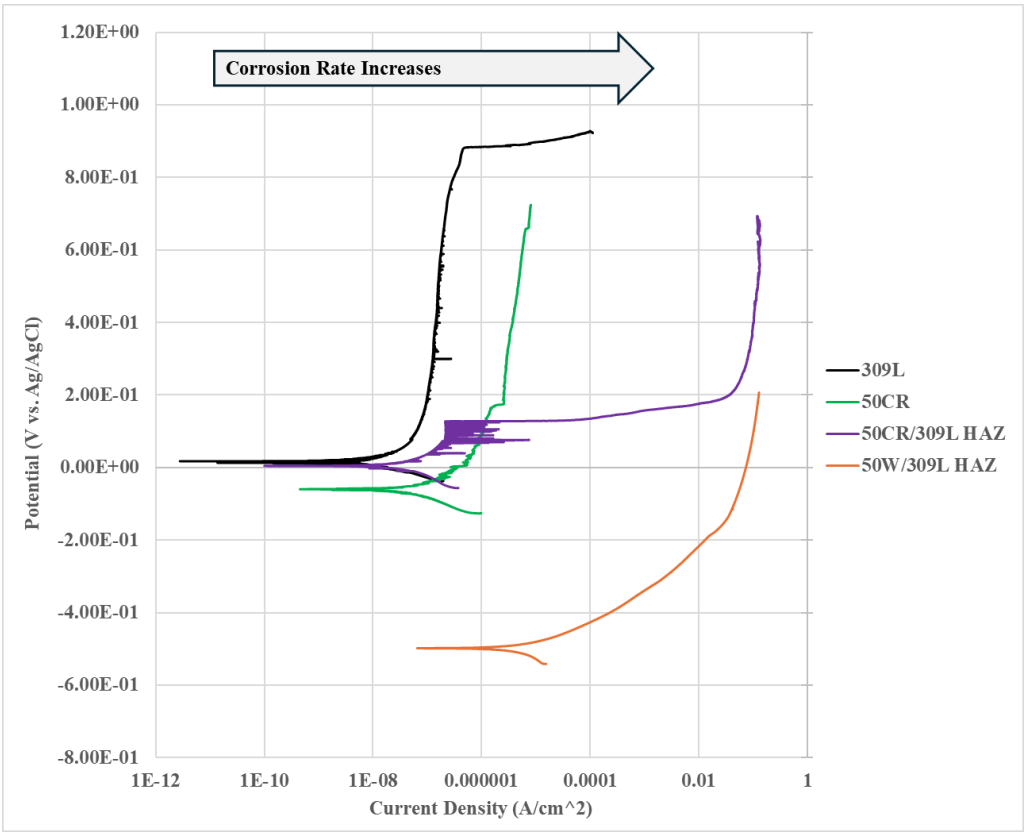

Figure 34. Anodic Polarization Scan Results Show the Relative Activity between the More Active 50W Steel Compared with the 50CR Steel and the Most Noble 309L Weld Metal. Pitting potentials are clearly shown as rapid increases in current density once a threshold voltage is reached for the stainless steels. HAZ = heat-affected zone.

Electrochemistry Testing: Potentiodynamic Polarization Measurements

After OCP tests, potentiodynamic scans were performed to assess the corrosion rate and determine the effects of galvanic corrosion on each of the base metals coupled with the 309L weld metal. Overlaying the individual anodic and cathodic scans can be used to estimate a galvanic corrosion rate, especially if OCP for the anode and cathode are more than 120 mV apart (ASTM International, 2022). Figure 35 shows these potentiodynamic scan results.

Table 11 shows the stable OCP for each of the base metals and the theoretical current density formed by the couple between the filler 309L. The nobility of each of the metals on its own decreases in the following order: 309L weld metal > 50CR steel > A36 steel > 50W steel. The estimated current density when each base metal is coupled with the 309L weld metal originates from the intersection point between the cathodic branch of the 309L weld metal polarization curve and the anodic branch of each base metal. The current density is proportional to the corrosion rate that would be expected if the base metal and 309L weld metal were physically attached in a galvanic couple. Based on this estimate of the galvanic corrosion rate, the corrosion resistance for the following dissimilar metal couples is 50CR steel/309L weld metal >> 50W steel/309L weld metal > A36 steel /309L weld metal.

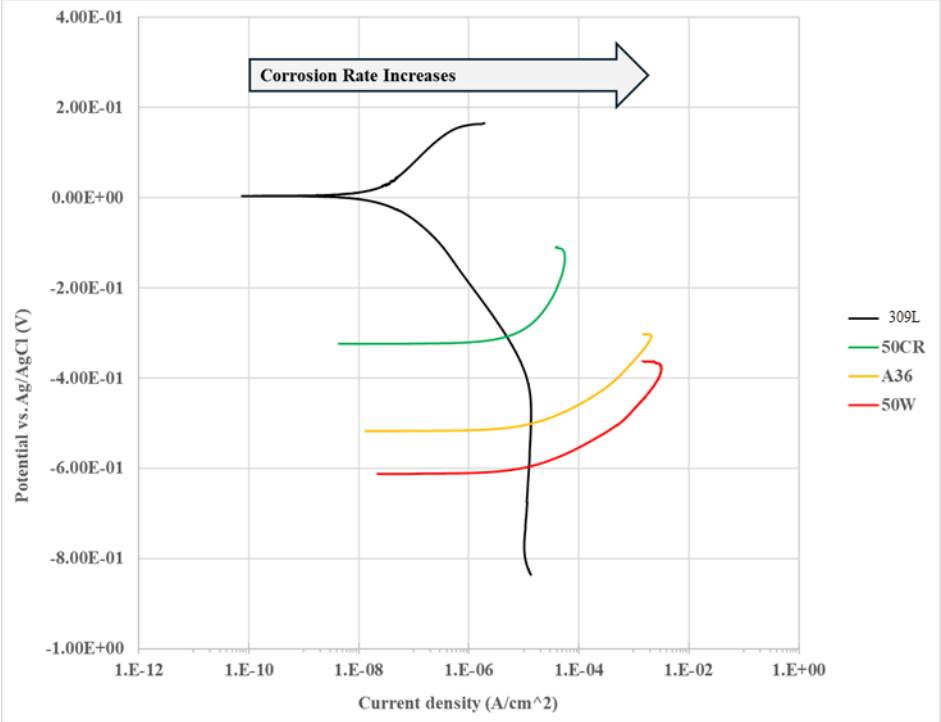

Figure 35. Potentiodynamic Scans for Each of the Base Metals. As seen in the comparison between each of the weld metals, the nobility of each of the metals decreases in the order of 309L weld metal > 50CR steel > A36 steel > 50W steel. The estimated current density for each of the couples, which is proportional to the corrosion rate, is lowest for 309L weld metal/50CR steel < 309L weld metal/50W steel < 309L weld metal/A36 steel.

Table 11. Open Circuit Potential and Current Density for Metal Coupled to 309L Weld Metal Based on Potentiodynamic Scans

Metal	Open Circuit Potential (Volts vs. Ag/AgCl)	Current Density Estimate when Metal Is Coupled to 309L Weld Metal (A/cm^2)
309L weld metal	– 0.0004	N/A
50CR steel	– 0.324	5.34e-6
50W steel	– 0.612	1.27e-5
A36 steel	– 0.517	1.35e-5

N/A = data not available.

In addition to measuring the corrosion behavior of each base metal and weld metal combination, corrosion initiation sites were explored to determine which areas began corroding first. This process was carried out by starting a potentiodynamic scan, applying an anodic current, and stopping it shortly afterward. These samples were then analyzed using SEM and EDS. Results showed that corrosion in the 50CR steel tended to initiate at impurities, with pits forming around slag inclusions found within the metal. Impurity inclusions are difficult to eliminate from commercially produced steel at industrial scales and are known to act as corrosion initiation sites for different metal alloys.

Electrochemistry Testing: Zero Resistor Ammeter Measurements

In addition to OCP and polarization testing, ZRA measurements were performed between each of the base metal and weld metal couples. Figure 36 shows these results. The A36/50W steels coupled to the 309L weld metal show a larger current value compared with the 50CR steel coupled to 309L weld metal. Because the current value is proportional to the corrosion rate, this function indicates that the A36 and 50W steels exhibit similar corrosion resistance, and the 50CR has a much slower corrosion rate, all when coupled to 309L weld metal.

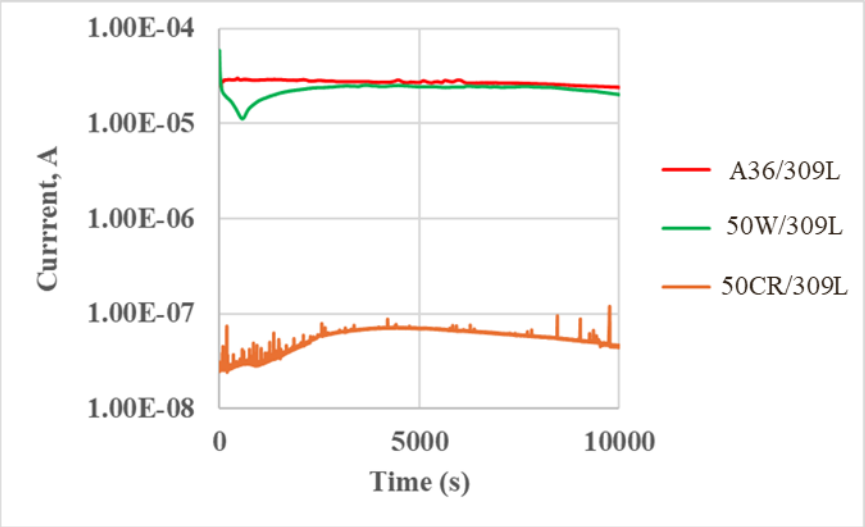

Figure 36. Zero Resistance Ammeter Measurements Made for Each of the Base Metals when Coupled to the 309L Weld Metal. The relatively stable voltage and current density for the A36 and 50W steels can be observed compared with the current density and voltage spikes observed for the 50CR steel because of the presence of metastable pits forming on the surface.

The current spikes on the 50CR steel plot are likely associated with localized pitting in steel compared with uniform corrosion. This association was expected because 50CR steel is alloyed for corrosion resistance. Although it is difficult to see in this semi-log plot, the A36 and 50W steels also exhibited current and potential spikes throughout the test. These drops are due to the formation and growth of metastable pits, which can begin to grow as local depassivation occurs on the surface and is then followed by repassivation, which stops the growth of the pit (Frankel, 1987). Ranking these alloys for galvanic corrosion based on ZRA measurements from greatest to least corrosion resistance yields the following: 50CR steel/309L weld metal >> 50W steel/309L weld metal > A36 steel/309L weld metal.

Chromium Concentration Sensitivity and Intergranular Attack

50CR steel, which is a higher chromium martensitic and ferritic stainless steel compared with the A36 and 50W carbon steels, showed minimal corrosion and a different corrosion morphology as well. Instead of showing uniform corrosion across the surface when a potential was applied, the 50CR steel resulted in pitting. These pits were large within the HAZ. However, outside the HAZ, the pits appeared to behave independently of the galvanic couple or thermally affected region and acted similarly to 50CR steel base metal.

Figure 37 shows an optical micrograph, SEM, and an EDS map of the distribution of pits close to the 309L weld metal interface. At the 309L weld metal interface, the pits were larger and spaced closely together. Moving away from the weld interface, the pits were smaller and spaced farther apart.

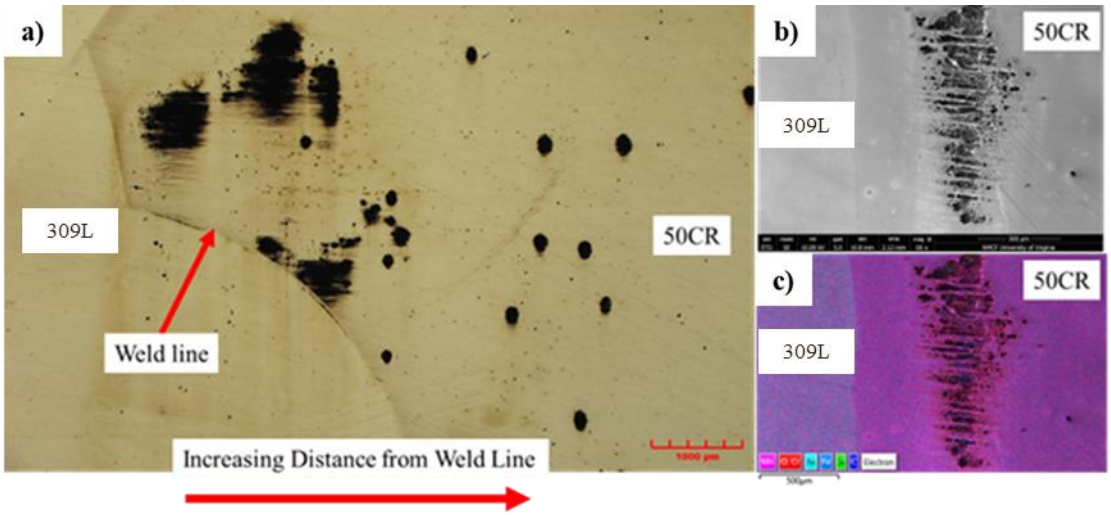

Figure 37. (a) Optical Micrograph Showing the Distribution of Pits and Distance away from the Weld Line where the Heat-Affected Zone Effects the Pit Formation and Morphology. (b) Scanning electron microscopy and (c) energy dispersive spectroscopy maps show detailed views of the large pits within the heat-affected zone of the 50CR steel.

On closer examination of the pits near the 50CR steel and 309L weld line, two phases were present in the HAZ with different chromium concentrations, which is seen in the corroded bands in the micrographs in Figure 37b and Figure 37c. These different phases had chromium concentrations of approximately 13.6% and 11.5% by weight. Although these differences are only slightly greater than the accuracy limits of EDS, they were consistent across multiple measurement sites. These differences were observed within both the HAZ and base metal (Figure 38). These two phases were also shown previously in the micrographs in Figure 15c and Figure 15d.

Although approximately 10.5% chromium is typically quoted as the required concentration necessary to form a passivating surface in stainless steels, it is also noted that 13% is known to provide significant corrosion resistance when alloyed with other corrosion-resisting elements. Chromium strongly influences corrosion rates, and therefore, small changes in its concentration can yield large effects on corrosion resistance (Kamimura and Stratmann, 2001). In addition, others have noted that the measured corrosion rates decrease as the chromium content increases from 5 to 11% in experimental steels (Fletcher, 2011).

When considering chromium concentration, some of the pits that formed during polarization were present in the 50CR steel just adjacent to the 309L weld interface. Figure 39 shows SEM and EDS line scans demonstrating the proximity to some of the pits formed along the interface with the 309L weld metal. As Figure 39 shows, pits were most prevalent at the weld interface in phases with less chromium concentration.

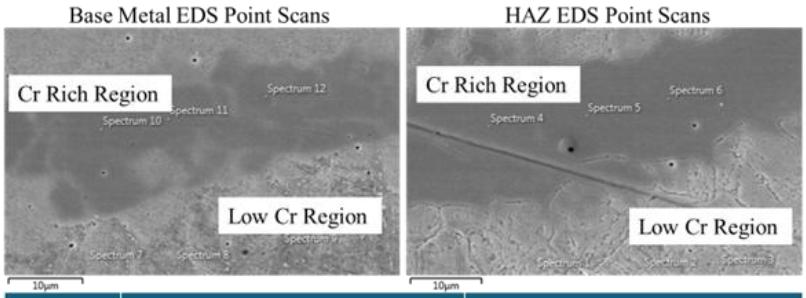

	Base Metal		Heat Affected Zone (HAZ)	
Point Scan	Low Cr Region	High Cr Region	Low Cr Region	High Cr Region
1	11.6	13.5	11.4	13.9
2	11.8	13.3	11.3	13.7
3	11.5	13.3	11.4	14.1
Average	11.64 wt.%	13.37 wt.%	11.37 wt.%	13.9 wt.%

Figure 38. Differences in Chromium Concentration Found between Two Different Phases in the 50CR Steel Results in the Unique Pitting Morphology Observed in the Heat-Affected Zone of the 50R Steel. EDS = energy dispersive spectroscopy.

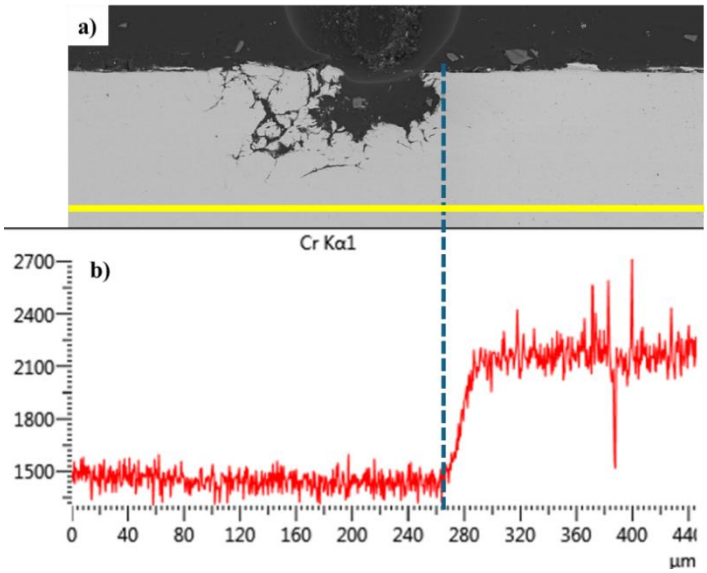

Figure 39. (a) Scanning Electron Microscopy Image with Overlaid Line Scan Profile (shown by the yellow line) where the Energy Dispersive Spectroscopy Line Scan Was Measured. (b) Chromium signal across the line profile showing the significant difference in chromium concentration between the 309L weld metal and 50CR steel.

In addition to the chromium segregation between the dual-phase microstructure in the 50CR steel, sensitization was observed within the phase containing less chromium. The 50CR steel was cross-sectioned after polarization to determine the effect of the HAZ microstructure on the corrosion pitting and growth. Large pits predominantly formed within the HAZ and showed signs of intergranular attack, which is indicative of sensitization.

Figure 40 shows optical micrographs of an etched cross section of a polarized and corroded 50CR steel sample, low magnification images showing the region in which pits form within the 50CR steel and high magnification images showing the grain boundary attack within

the pits. This scenario is commonly observed in sensitized metals, in which chromium depletion around grain boundaries leads to increased corrosion rates between grains, which appears as grain boundary attack (Amuda and Mridha, 2011). Welding is especially known to cause sensitization in stainless steels because of the cyclic reheating that occurs during the welding process (Dahmen et al., 2015).

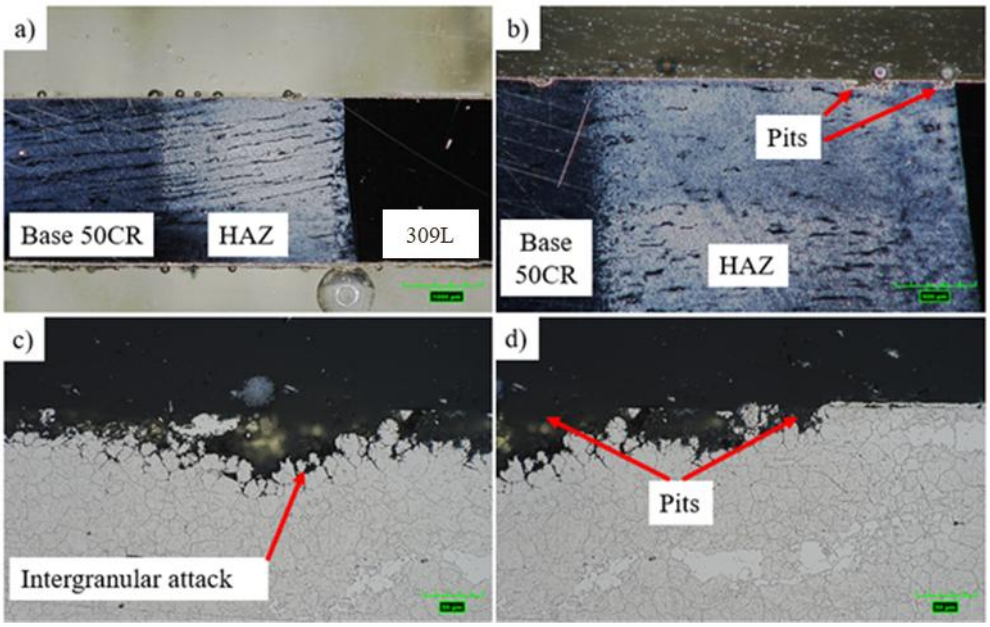

Figure 40. (a) and (b) Optical Micrographs of an Etched Cross Section Showing the HAZ within the 50CR Steel and the Location of Pitting. (c) and (d) High magnification images of the intergranular corrosion due to the sensitization that occurs within the HAZ. HAZ = heat-affected zone.

Summary of Corrosion Testing

Four different types of corrosion were observed in the bae metals and HAZs of the DMWs: uniform, pitting, galvanic, and intergranular. In terms of base metals, the A36 and 50W steels showed uniform corrosion, whereas the 50CR steel showed pitting corrosion and local attack. The corrosion resistance of the bulk materials from greatest to least corrosion resistance was 309L weld metal >> 50CR steel >> 50W steel > A36 steel.

Distinct corrosion morphologies were observed in the HAZ for the 50CR, 50W, and A36 steels at the 309L weld metal interface due to the distinct microstructures in these regions. Galvanic corrosion in the A36 and 50W steel HAZs caused them to corrode at an accelerated rate compared with A36 and 50W steel base metals. Galvanic corrosion in the 50CR steel HAZ caused deeper and more concentrated pits compared with the 50CR base metal. Pitting corrosion in the 50CR steel HAZ was observed where the chromium concentration was decreased, and intergranular attack, known as sensitization, also occurred. Slag impurity inclusions within the 50CR steel were found to be initiation sites for pitting within both the HAZ and base metal. The corrosion resistance of the HAZ samples from greatest to least corrosion resistance was 50CR steel/309L weld metal >> 50W steel/309L weld metal > A36 steel/309L weld metal.

Nondestructive Evaluation Examination

Ultrasonic Wave Velocity Testing

Figure 41 shows how the ultrasonic wave velocity changed with temperature for the different types of steel samples (50CR steel, 412 steel, A36 steel, and pure 309L weld metal). In all cases, the wave velocity decreased as the temperature increased. This occurrence highlights the need to perform UT calibration on a calibration block at the same temperature as the test object to ensure accurate results.

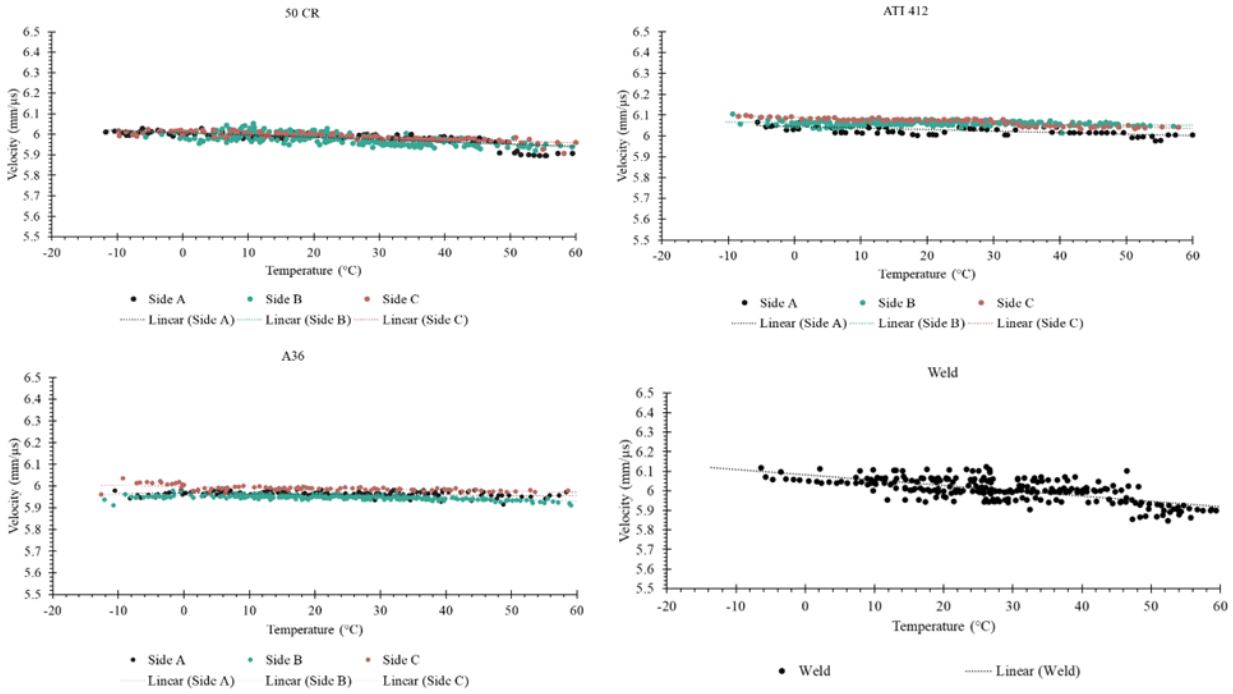

Figure 41. Ultrasound Wave Velocity Change with Temperature for Different Steels and Pure 309L Weld Metal. ATI 412 = 412 steel; 50CR = 50CR steel; A36 = A36 steel.

The degree of velocity change with temperature varied among materials. The 50CR and 412 steels were slightly more sensitive to temperature than A36 steel. The pure 309L weld metal showed the greatest variation, likely because of its mixed phases, residual stresses, and mixed microstructure.

When wave velocity was measured in all three directions for each sample, some materials showed directional differences, known as anisotropy, especially the 412 steel. This behavior is linked to the microstructure of the 412 steel. For example, the microstructure of the 412 steel has layers of ferrite and tempered martensite, similar to the layers seen in Figure 15 for 50CR steel, which causes ultrasound to travel at different speeds depending on whether it moves parallel or perpendicular to these layers. For this reason, calibration is most reliable when using a block of the same material and aligned with the test surface.

Phased Array Ultrasonic Testing

PAUT was performed on all NDE specimens from two directions: from the 50CR steel toward carbon steel and from the carbon steel toward 50CR steel, corresponding to Sides A and B, respectively. When scanning from Side A, most defects in the base metals were successfully detected and located with acceptable accuracy. However, most of the stacked defects at the weld center were not detected, except for the one at the bottom of the plate (Figure 42). This difference is due to beam behavior. Defects in the base metal did not cause significant skew, whereas defects in the weld metal required the ultrasonic beam to pass through two dissimilar materials, introducing refraction and skewness that reduced detectability.

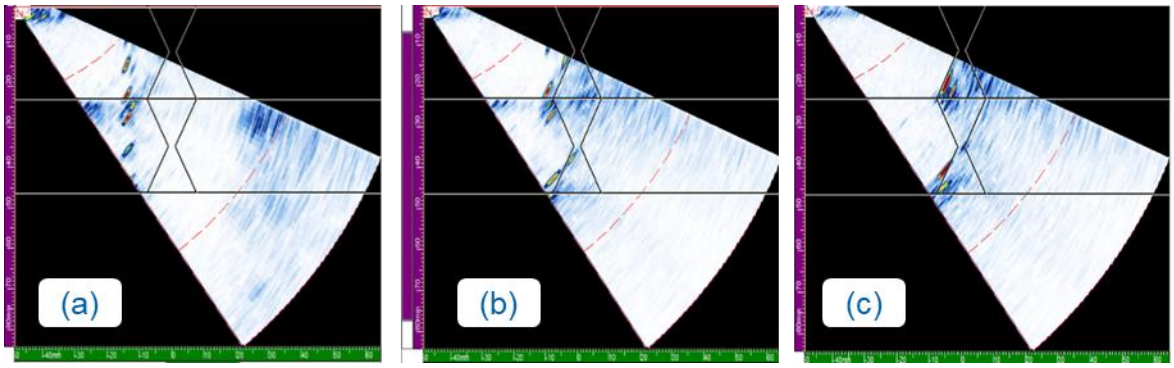

Figure 42. Phased Array Ultrasonic Testing Results of Specimen Nondestructive Evaluation-1: (a) Scan on Side A from 50CR Steel toward Carbon Steel; (b) Scan on Side B from 50CR toward Carbon Steel; (c) Scan on Side B from Carbon Steel Toward 50CR Steel

When scanning from Side B with the probe directed from the 50CR steel toward the carbon steel, only two defects at the weld boundary on the 50CR steel side and one defect near the weld center were detected (Figure 42). The central defect was close to the 50CR steel weld interface, indicating a horizontal shift in defect positioning. Defects on the carbon steel side were completely missed during inspection. Conversely, when scanning from the carbon steel toward the 50CR steel, defects in the carbon steel were consistently detected, whereas those defects in the 50CR steel were not. In this case, the central weld defect was more accurately detected at the weld center. The sound beam skew in these cases was measured to be approximately 0.2 inch.

Overall, these results demonstrate that material mismatch and beam refraction at the DMW interface have a significant effect on defect detectability. To minimize the risk of missed flaws and improve inspection reliability, welds must be evaluated from both sides whenever possible.

Based on this finding, specimen NDE-3 was tested using a dual-probe system (Figure 43a). This configuration demonstrated good potential for detecting all defects in a single pass of the probes parallel to the weld, thereby improving inspection efficiency (Figure 43b). However, the approach had some limitations. First, sufficient clearance was required on both sides of the weld to allow the probe assembly to move along the weld direction, which may not always be feasible in field applications. Second, surface roughness hindered smooth probe movement, which occasionally caused displacement of the probe, reducing the accuracy of both defect detection and localization.

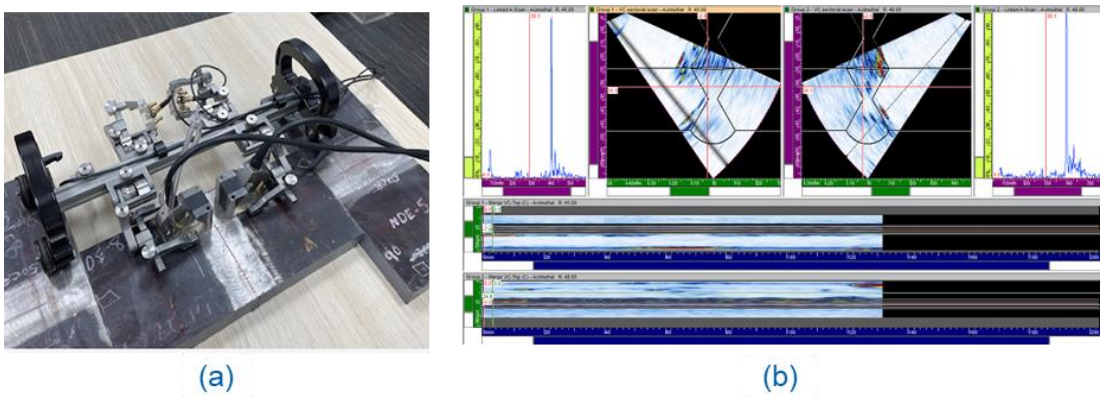

Figure 43. Dual-Probe System: (a) Configuration of Two-Side Data Acquisition; (b) Collected Data near Side B.

In addition to the side-drilled holes, the surface notches introduced in the carbon steel, 50CR steel, and 309L weld regions were examined using PAUT. These notches were not detected in either the A-scan or S-scan; however, they were identified in the C-scan (Figure 44). This outcome suggests that shallow cracks may be easily missed during PAUT inspection if the inspector focuses only on a single view or scan window. For this reason, special attention is required when evaluating welds, and using complementary techniques such as ACFM should be considered to improve reliability.

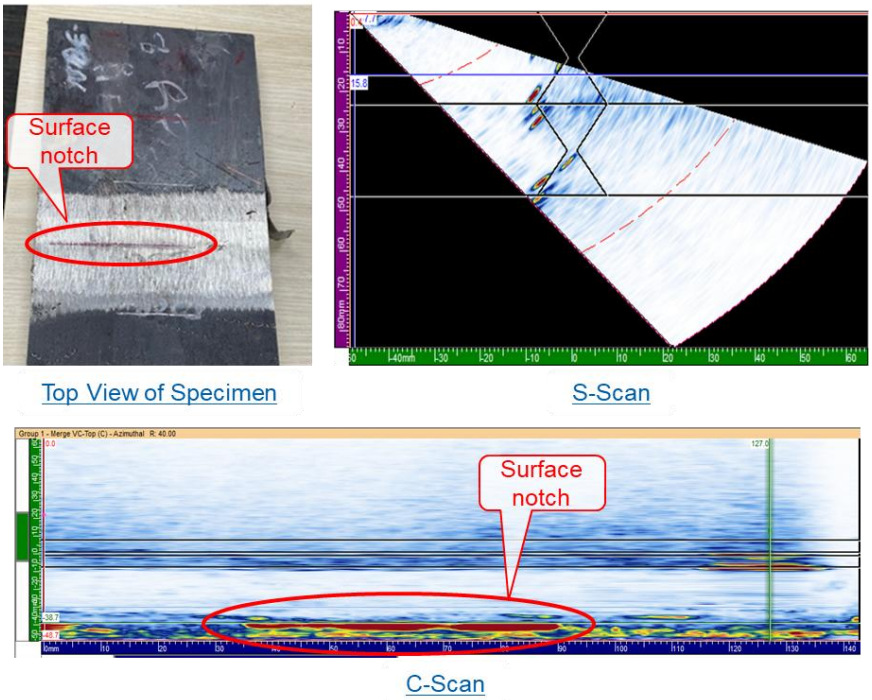

Figure 44. Notch Detection with Phased Array Ultrasonic Testing

Using a longitudinal dual matrix probe significantly reduced the skew of the ultrasonic wave, which also improved the signal-to-noise ratio. As Figure 45 shows, this enhancement allowed for more accurate detection of defects not only within the weld but also on the opposite

side of the joint. By reducing beam distortion, the probe provided better resolution and more reliable results, ensuring that even subtle or deeper defects were detected, which might otherwise be missed with conventional probes. The longitudinal dual matrix probe optimizes beam focusing, ensuring that the sound wave remains more directed and consistent as it travels through the material. This characteristic is crucial when inspecting critical welds, where small variations in defect position or orientation can alter the effectiveness of traditional inspection techniques. Furthermore, the improved signal-to-noise ratio enabled more accurate data interpretation.

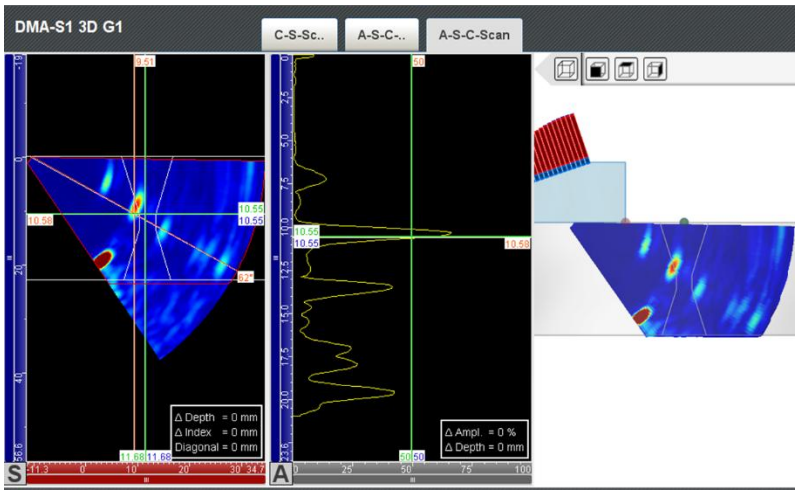

Figure 45. Improved Defect Detection Using Longitudinal Wave Probe

Alternating Current Field Measurement Testing

Because cracks can be present on weld surfaces or interfaces, and PAUT did not provide depth information, ACFM was evaluated as an alternative technique for detecting shallow cracks. The results shown in Figure 46 confirm that ACFM performed effectively on the carbon steel side, successfully detecting and measuring the shallow surface defect (in this case, the notch simulating a crack). However, no signals were obtained for the weld metal or the 50CR steel. This limitation arises because ACFM relies on the generation of a magnetic field, and both the weld and 50CR steel are stainless steels, meaning they cannot support magnetic flux transfer. These findings suggest that ACFM could serve as a rapid and reliable alternative to magnetic particle testing for surface defects in carbon steel weld regions. The technique is also advantageous because data acquisition is fast, and interpretation requires minimal training.

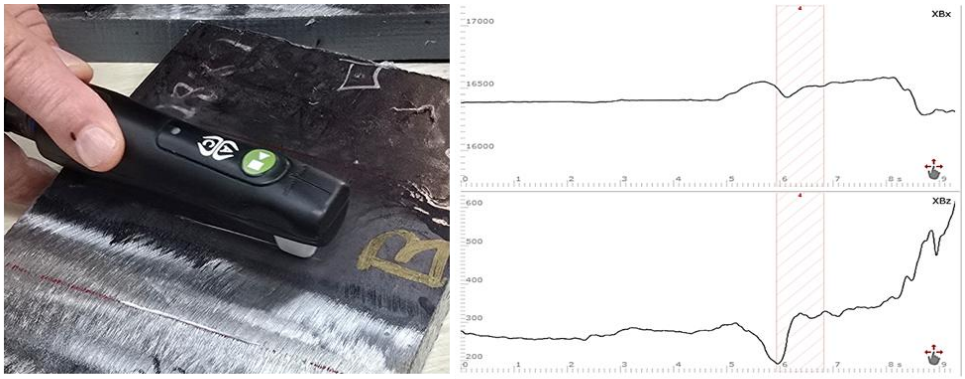

Defects

	Length (in)	Depth (in)	Rows	Location (smpl)	Coat (in)	CF	Field
4	1.913	0.014	1	1187 .. 1365	0.000	1.45	X

Figure 46. Alternating Current Field Measurement Test Results on a Notch

Summary of Findings

- *412 steel has similar corrosion resistance and mechanical properties to 50CR steel and is produced on a regular basis by a domestic steel supplier. However, 412 steel does not meet the ASTM A709 Grade 50CR specifications because it is produced using a different heat treatment process compared with 50CR steel. Therefore, if 412 steel were to be specified on a future steel bridge project, a material specification for the steel would need to be developed.*

- *Dissimilar metal groove welds made with 50CR/412 steel and typical bridge steels, such as either A36 or 50W steel, were susceptible to solidification cracking and cold cracking when welded with the welding parameters used for typical steel bridge welds.*

- *Dissimilar metal groove welds made with 50CR/412 steel and A36/50W steel can be successfully welded using lower heat input and a single-V with backgouge weld joint. These welding parameters alleviated both solidification cracking and cold cracking.*

- *In addition to using a lower heat input and a single-V with backgouge joint, dissimilar metal groove welds made with 412 steel and A36/50W steel using the SAW process need to use a 309L cored filler metal to prevent cracking.*

- *Crack-free dissimilar metal groove welds made with 50CR/412 steel and A36/50W steel can meet the mechanical property requirements of the AASHTO/AWS D1.5 Bridge Welding Code.*

- *DMWs made with 50CR/412 steel and A36/50W steel experienced uniform, pitting, galvanic, and intergranular corrosion.*

- *Galvanic corrosion in DMWs made with 50CR/412 steel and A36/50W steel experienced an accelerated corrosion rate of the HAZs on both sides of the stainless steel weld interface. The A36/50W steel HAZ experienced an accelerated uniform corrosion rate compared with*

A36/50W steel base metal, and the 50CR steel HAZ experienced an accelerated pitting and intergranular corrosion rate compared with 50CR steel base metal.

- *Pitting in the 50CR steel HAZ of DMWs made with 50CR/412 steel and A36/50W steel occurred in areas of low chromium concentrations. In addition, slag impurity inclusions in the 50CR steel were found to be initiation points for pitting corrosion both within the HAZ and the base metal.*

- *The corrosion resistance of the HAZs from DMWs made with 50CR steel and A36/50W steel from greatest to least corrosion resistance was 50CR steel/309L weld metal >> 50W steel/309L weld metal > A36 steel/309L weld metal.*

- *RT using the parameters typically used for steel bridge welds was not always effective at identifying defects in DMWs made with 50CR/412 steel and A36/50W steel. Some radiographic test results in this project could identify defects, and others showed artifacts that could easily mask potential defects, causing them to be undetected.*

- *Because of ultrasonic anisotropic behavior, meaning having different properties in different directions, the traditional calibration procedures for UT and PAUT, as specified by the AASHTO/AWS D1.5 Bridge Welding Code, lead to mislocating defects in 50CR steel, 412 steel, and 309L weld metal. Instead, calibration needs to be performed using a calibration block made from the same materials, including base metals and weld metal, and with the rolling direction of all materials oriented in the same direction as the production piece.*

- *Because of ultrasonic wave refraction, the traditional test parameters used for UT and PAUT, as specified by the AASHTO/AWS D1.5 Bridge Welding Code, lead to completely missing or mislocating defects in DMWs made from 50CR/412 steel and A36/50W steel. Ultrasonic wave refraction can be accounted for in the base metals of these welds by scanning the weld from both sides; however, defects within the 309L weld metal can be completely undetected or located inaccurately.*

- *ACFM testing was able to effectively locate and measure surface cracks on the carbon steel side of the DMWs.*

CONCLUSIONS

- *DMWs made between 50CR/412 steel and 50W/A36 steel can meet the mechanical property requirements of the AASHTO/AWS D1.5 Bridge Welding Code.* This standard requires using different welding parameters than those typically used for other steel bridge welds.

- *DMWs made with 50CR/412 steel and A36/50W steel experience a significant reduction in corrosion resistance compared with non-dissimilar 50CR steel welds and the base metals in these welds.* The HAZs of the welds and the base metals experience multiple forms of detrimental corrosion, including uniform, pitting, galvanic, and intergranular corrosion. The corrosion resistance of the HAZs in these DMWs is, from greatest to least corrosion

resistance, 50CR steel/309L weld metal >> 50W steel/309L weld metal > A36 steel/309L weld metal.

- *Significant challenges remain with the NDE of DMWs made with 50CR/412 steel and A36/50W steel.* RT using parameters typically used for other bridge welds has the potential to mask potential defects in these DMWs. Because of the ultrasonic anisotropy of DMWs, defects in the welds can be missed or mislocated using traditional UT calibration processes. Furthermore, ultrasonic wave refraction can lead to missing or mislocating defects in these welds when inspecting them using traditional UT or PAUT.

- *412 steel is a potential alternative to 50CR steel.* 412 steel has similar chemistry to 50CR steel, giving it similar corrosion resistance, has similar mechanical properties to 50CR steel, and is regularly produced by a domestic steel supplier. However, it does not meet the current heat treatment requirements for Grade 50CR steel as specified in ASTM A709.

- *ACFM testing has the potential to be used as a reliable technique for detecting surface defects in typical carbon steel bridge welds.*

RECOMMENDATIONS

1. *The VDOT Structure and Bridge Division should not pursue using 50CR/412 steel in DMWs.* Although this project was successful at identifying the welding parameters necessary to fabricate crack-free DMWs meeting the mechanical property requirements of the AASHTO/AWS D1.5 Bridge Welding Code, significant challenges remain with the corrosion performance and NDE of these DMWs. It is possible that future research could identify solutions to these challenges, but until both are resolved, such DMWs should not be used on steel bridges.

2. *The VDOT Structure and Bridge Division should continue to exercise caution when specifying 50CR steel on bridges because of the recent poor quality and long lead times of the 50CR steel*. If the 50CR steel supplier remedies these challenges, then VDOT could consider expanding its use. If a bridge project requires the inherent corrosion resistance of 50CR steel but the supplier has not yet solved the quality and lead time challenges, VDOT could consider using 412 steel.

IMPLEMENTATION AND BENEFITS

The researchers and the technical review panel (listed in the Acknowledgments) for the project collaborate to craft a plan to implement the study recommendations and determine the benefits of doing so. This process is to ensure that the implementation plan is developed and approved with the participation and support of those involved with VDOT operations. The implementation plan and the accompanying benefits are provided here.

Implementation

Based on the remaining challenges with the corrosion performance and NDE of DMWs with 50CR/412 steel, specifications for these welds will not be incorporated into VDOT's existing guidance on the use of 50CR steel. Therefore, no implementation action items are necessary for Recommendation 1.

VDOT has paused the use of 50CR steel due to quality and lead time challenges with the steel supplier. Using 412 steel on a bridge project would require new guidance on its use because 412 steel does not meet the heat treatment requirements of ASTM A709 Grade 50CR steel. If a project arises that would benefit from using 412 steel, the VDOT Structure and Bridge Division, VDOT Materials Division, and the Virginia Transportation Research Council (VTRC) will work together to develop a special provision for specifying 412 steel. Once a project has demonstrated successful use of 412 steel, specifications for 412 steel may be incorporated into VDOT's existing guidance on using 50CR steel. Therefore, at this time, no implementation action items are necessary for Recommendation 2.

Benefits

Both recommendations allow VDOT to proactively manage risks on future projects. Not using DMWs ensures structural integrity because these welds have reduced durability and have the potential to include defects even after shop inspection. Exercising caution on using 50CR steel supports VDOT's commitment to reliable project delivery, helping ensure that projects are completed on time and on budget. VDOT previously incurred approximately $1.0 million in costs because of challenges with 50CR steel. Exercising caution on its use in future projects reduces the likelihood of similar financial losses.

ACKNOWLEDGMENTS

The authors are thankful to the following individuals who served on the technical review panel for this study: Adam Matteo, Project Champion, VDOT Structure and Bridge Division; Jeremy Clary, VDOT Materials Division; Junyi Meng, VDOT Structure and Bridge Division; Ed Darby, VDOT Structure and Bridge Division; and Justin Ocel, Federal Highway Administration. The authors also acknowledge former technical review panel members Christine Fuller, formerly of VDOT Hampton Roads District, and Jhony Habbouche, formerly of VTRC. The authors also thank Soundar Balakumaran, formerly of VTRC; John "Michael" Epperson, formerly of VTRC; Graham Frazier, VTRC; Adrian Blackstone, VTRC; and Susan Warr, VDOT Richmond District.

REFERENCES

Alcantar-Modragon, N., Garcia-Garcia, V., Reyes-Calderon, F., Villalobos-Brito, J.C., and Vergara-Hernandez, H.J. Study of Cracking Susceptibility in Similar and Dissimilar Welds Between Carbon Steel and Austenitic Stainless Steel Through Finger Test and FE

Numerical Model. *The International Journal of Advanced Manufacturing Technology*, Vol. 116, July 2021, pp. 2661–2686.

American Association of State Highway and Transportation Officials and American Welding Society. *Bridge Welding Code*. Washington, DC, 2020.

American Society of Mechanical Engineers. *ASME Boiler and Pressure Vessel Code (2017) Section V: Nondestructive Examination*. New York, 2017.

ASTM International. *ASTM G82-98(2021): Standard Guide for Development and Use of a Galvanic Series for Predicting Galvanic Corrosion Performance*. West Conshohocken, PA, 1981.

ASTM International. *ASTM G1: Standard Practice for Preparing, Cleaning, and Evaluating Corrosion Test Specimens*. West Conshohocken, PA, 2017.

ASTM International. *ASTM G71-81(2019): Standard Guide for Conducting and Evaluating Galvanic Corrosion Tests in Electrolytes*. West Conshohocken, PA, 2019.

ASTM International. *ASTM G5-14(2021): Standard Reference Test Method for Making Potentiodynamic Anodic Polarization Measurements*. West Conshohocken, PA, 2021a.

ASTMs International. *ASTM A709/A709M-21: Standard Specification for Structural Steel for Bridges*. West Conshohocken, PA, 2021b.

ASTM International. *Supplement to Corrosion Tests and Standards: Application and Interpretation, 2nd edition*. West Conshohocken, PA, 2022.

Amuda, M.O.H., and Mridha, S. An Overview of Sensitization Dynamics in Ferritic Stainless Steel Welds. *International Journal of Corrosion*, July 2011, pp. 1–9.

Chassignole, B., Dupond, O., Doudet, L., Duwig, V., and Etchegaray, N. Ultrasonic Examination of an Austenitic Weld: Illustration of the Disturbances of the Ultrasonic Beam. In *American Institute of Physics Conference Proceedings*, AIP Publishing, Chicago, IL, 2009, pp. 1886–1893.

Connor, R.J., Schroeder, C.J., Crowley, B.M., Washer, G.A., and Fish, P.E. *Acceptance Criteria of Complete Joint Penetration Steel Bridge Welds Evaluated Using Enhanced Ultrasonic Methods*. No. 908. Transportation Research Board, Washington, DC, 2019.

Dahmen, M., Rajendran, K.D., and Lindner, S. Sensitization of Laser-Beam Welded Martensitic Stainless Steels. *Physics Procedia*, Vol. 78, December 2015, pp. 240–246.

Easterling, K. *Introduction to the Physical Metallurgy of Welding, 2nd edition.* Butterworth-Heinemann Elsevier, Oxford, UK, 1992.

Edelmann, X. Application of Ultrasonic Testing Techniques on Austenitic Welds for Fabrication and In-Service Inspection. *NDT International*, Vol. 14, No. 3, June 1981, pp. 125–133.

Edelmann, X. Ultrasonic Examination of Austenitic Welds at Reactor Pressure Vessels. *Nuclear Engineering and Design*, Vol. 129, No. 3, August 1991, pp. 341–355.

Esfahani, M.N. *Laser Welding of Dissimilar Carbon Steel to Stainless Steel 316L*. Ph.D. dissertation. Loughborough University, London, UK, 2015.

Fitz-Gerald, J.M., Agnew, S.R., and Xia, X. *Welding of ASTM A709 50CR Using Austenitic Filler Wires with Varying Heat Inputs and Maximum Interpass Temperatures*. VTRC-20-R24. Virginia Transportation Research Council, Charlottesville, VA, 2020.

Fletcher, F.B. *Improved Corrosion-Resistant Steel for Highway Bridge Construction*. FHWAHRT-11-062. Federal Highway Administration, Washington, DC, 2011.

Frankel, G.S., Stockert, L., Hunkeler, F., and Boehni, H. Metastable Pitting of Stainless Steel. *Corrosion*, Vol. 43, No. 7, July 1987, pp. 429–436.

Groshek, I.G., and Hebdon, M.H. Galvanic Corrosion of ASTM A1010 Steel Connected to Common Bridge Steels. *Journal of Materials in Civil Engineering*, Vol. 32, No. 8, May 2020.

Han, T., Schubert, F., Hillmann, S., and Meyendorf, N. Phased Array Ultrasonic Testing of Dissimilar Metal Welds Using Geometric-Based Referencing Delay Law Technique. In *Smart Materials and Nondestructive Evaluation for Energy Systems*. SPIE, San Diego, CA, 2015, pp. 15–25.

Hebdon, M.H., and Provines, J.T. The Use of ASTM A1010 (A709 GR50CR) Stainless Steel for Bridges in the United States. *Journal of Performance of Constructed Facilities*, Vol. 34, No. 6, August 2020.

International Organization for Standardization. *ISO 16811:2012: Non-destructive Testing—Ultrasonic Testing—Sensitivity and Range Setting*. Geneva, Switzerland, 2012.

Kamimura, T., and Stratmann, M. The Influence of Chromium on the Atmospheric Corrosion of Steel. *Corrosion Science*, Vol. 43, No. 3, March 2001, pp. 429–447.

Khan, W.N., and Chhibber, R. Effect of Filler Metal on Solidification, Microstructure and Mechanical Properties of Dissimilar Super Duplex/Pipeline Steel GTA Weld. *Materials Science and Engineering: A*, Vol. 803, October 2020.

Khorrami, M.S., Mostafaei, M.A., Pouraliakbar, H., and Kokabi, A.H. Study on Microstructure and Mechanical Characteristics of Low-Carbon Steel and Ferritic Stainless Steel Joints. *Materials Science and Engineering: A*, Vol. 608, 2014, pp. 35–45.

Kumar A., Sasi, B., Sharma, G.K., Rao, B.P., and Jayakumar, T. Nondestructive Evaluation of Austenitic Stainless Steel Welds. *Advanced Materials Research*, Vol. 794, September 2013, pp. 366–374.

Lottes, S.A., and Bojanowski, C. *Computer Modeling and Analysis of Truck-Generated Salt Spray Transport Near Bridges*. ANL/ESD/13-1. Argonne National Laboratory, Argonne, IL, 2013.

Murat, M.G., and Basyigit, A.B. The Effects of TIG Welding Rod Compositions on Phase Distributions and Corrosion Properties of Dissimilar 304L and 420 Stainless Steel Welds. *International Journal of Engineering Research and Development*, Vol. 12, No. 1, January 2020, pp. 134–147.

Nageswaran, C., Carpentier, C., and Tse, Y. Microstructural Quantification, Modelling and Array Ultrasonics to Improve the Inspection of Austenitic Welds. *Insight—Non-Destructive Testing and Condition Monitoring*, Vol. 51, No. 12, December 2009, pp. 660–666.

Okonkwo, B., Ming, H., Wang, J., and Han, E. Galvanic Corrosion Study Between Low Alloy Steel A508 and 309/308 L Stainless Steel Dissimilar Metals: A Case Study of the Effects of Oxide Film and Exposure Time. *Journal of Nuclear Materials*, Vol. 548, February 2021.

Okonkwo, B., Ming, H., Zhang, Z., Wang, J., Rahimi, E., Saman, H., and Davoodi, A. Microscale Investigation of the Correlation Between Microstructure and Galvanic Corrosion of Low Alloy Steel A508 and its Welded 309/308L Stainless Steel Overlayer. *Corrosion Science*, Vol. 154, April 2019, pp. 49–60.

Provines, J.T., Ocel, J., Harrop, K., Darby, T., Sharp, S.R., and Moruza, A.K. Analysis and Construction of the United States' First Completely Stainless Steel Bolted Splice on a Steel Girder Highway Bridge. In *Conference Proceedings of the World Steel Bridge Symposium*. National Steel Bridge Alliance, Baltimore, MD, 2018.

Provines, J.T., Sharp, S.R., and Moruza, A.K. *Documentation and Evaluation of ASTM A709 Grade 50CR Steel Bridges on Virginia's Eastern Shore*. VTRC 24-R2. Virginia Transportation Research Council, Charlottesville, VA, 2023.

SAE International. *SAE J2334 Laboratory Cyclic Corrosion Test*. Warrendale, PA, 2016. https://www.sae.org/standards/content/j2334_201604/.

Schroeder, C.J., Connor, R.J., Crowley, B.M., and Washer, G.A. Acoustic Properties of Steel Bridge Base Metals. *Research in Nondestructive Evaluation*, Vol. 32, November 2021, pp. 238–262.

Seradj, H. Oregon's ASTM A1010 Bridges. Presented at Iowa DOT A1010 Steel Workshop. Iowa Department of Transportation, Ames, IA, March 18, 2015.

Sharp, S.R., Provines, J.T., Moruza, A.K., Via Jr., W.F., and Harrop, K.N. Design, Fabrication, Construction, and Cost Assessment of Virginia's First Corrosion-Resistant ASTM A1010 Plate Girder Bridge. *Transportation Research Record*, Vol. 2672, No. 26, June 2018, pp. 68–76.

Sharp, S.R., Provines, J.T., Moruza, A.K., Via Jr., W.F., and Harrop, K.N. *Virginia's First Corrosion-Resistance ASTM A1010 Plate Girder Bridge.* FHWA/VTRC 20-R10. Virginia Transportation Research Council, Charlottesville, VA, November 2019. http://www.virginiadot.org/vtrc/main/online_reports/pdf/20-r10.pdf.

Szklarska-Smialowska, Z. *Pitting and Crevice Corrosion*. NACE International, Houston, TX, 2005.

Taraphdar, P., Kumar, R., Giri, A., Pandey, C., Mahapatra, M., and Sridhar, K. Residual Stress Distribution in Thick Double-V Butt Welds with Varying Groove Configuration, Restraints and Mechanical Tensioning. *Journal of Manufacturing Processes*, Vol. 68, July 2021, pp. 1405–1417.

Vamsi Krishna, K., Rowthu, S., Nadakuduru, V.N., Pilla, G., and Kishore Babu, N. Effect of Welding Speed and Postweld Heat Treatment on Microstructural Characterization and Mechanical Properties of Gas Tungsten Arc Welded Ti-15V-3Al-3Cr-3Sn Joints. *Fusion Science and Technology*, Vol. 80, No. 1, January 2024, pp. 68–81.

Virginia Department of Transportation. *Virginia Test Methods*. Richmond, VA, 2018.

Zhang, J., Ebrahimi, N., and Lai, D. Galvanic Corrosion Risk of Using Galvanized A325 Bolts in Corrosion-Resistant Steel Bridges. *Journal of Bridge Engineering*, Vol. 24, No. 6, June 2019.

Zhang, Y., and Tian, L. The Effect of Joint Configuration on Residual Stress and Distortion of the 304 Stainless Steel Multi-Pass Welded Joints. *Materials Today Communications*, Vol. 30, March 2022.